https://doi.org/10.15255/KUI.2024.036
KUI-10/2025
Original scientific paper
Received August 25, 2024
Accepted November 4, 2024

Metavalent Bonds in Dimers of Metallic Elements within Biomacromolecules: Database-forming Approaches, Additionally Exemplified by Silver and Potassium Data

R. Kiralj *

Bjelovar University of Applied Sciences, Trg Eugena Kvaternika 4, 43 000 Bjelovar, Croatia

Abstract

Metallic homonuclear dimers exist in diverse forms, including as parts of biomacromolecular structures. The aim of this study was to identify all metallic elements forming such dimers in the Protein Data Bank (PDB), to rationalise dimer structure and bonding using various structural descriptors and statistical methods, and to support new findings with two additional studies on silver and potassium clusters. In total, 31 metals were identified as forming 565 dimers in crystal structures of biomacromolecules: *s*-block metals (Li, Na, Mg, K, Ca, Rb. Sr, Cs and Ba), transition metals (V, Mn, Fe, Co, Ni, Cu, Zn, Mo, Ru, Rh, Pd, Ag, Cd, Au and Hg), *p*-block metals (Ga, Tl and Pb), and lanthanides (La, Eu, Dy and Ho). These findings strongly suggest that any metal can form dimers within biomacromolecules. The identified dimers exhibit metavalent, or borderline metavalent/covalent, or metavalent/metallic bonding. In the PDB and other structural databases and literature sources, 761 silver clusters of all sizes were identified and analysed in terms of bonds *per* atom – bond length deviation relationship. Metavalent bonds or borderline metavalent/covalent or metavalent/metallic bonds exist in silver dimers and smaller clusters, whereas metallic bonding is predominant in larger clusters. Such or similar behaviour is expected for other metals. Partial atomic charge – radius relationship for 515 potassium clusters, from the PDB and other databases and sources, indicates that potassium dimers in biomacromolecules exhibit metavalent bonds or at least borderline metavalent/covalent or metavalent/metallic bonds, as demonstrated by the transferred electrons – shared electrons scatterplot. This behaviour is highly probable in other metals as well.

Keywords

Homonuclear metal dimers, biomacromolecular structures, metavalent bonding, statistical analysis, bonds per atom – bond length deviation relationship, atomic charge – radius relationship, transferred electrons – shared electrons relationship

Men put an end to darkness, and search out to the farthest bound the ore in gloom and deep darkness. (Job 28:3)

1 Introduction

The simplest metallic homonuclear clusters are dimers which exist in diverse forms: for instance, the Hg_2^{2+} cation in the condensed state,[1] the Au_2^{4+} cation in crystalline $AuSO_4$,[2] the Na_2 molecule in the gas phase,[3] the Rh_2^{4+} unit of catalyst molecule $Rh_2(O_2CR_4)$ (R = 2,4,6-triisopropyl benzoate) in the condensed state,[4] the K_2^{2-} anion in crystalline potassium cryptate potasside $K^+(C222)K^-$,[5] the Zn_2^{4+} cofactor unit at the active site of *Escherichia coli* periplasmic 5′-nucleotidase,[6] and the Fe_2^{4+} unit of the Fe_2S_2 cofactor in [FeFe]-hydrogenases,[7] among others. Metals are indeed an important subject in bioinorganic chemistry, yet special attention is not regularly given to metallic dimers or larger metallic clusters, their structure, bonding, and formation in biomacromolecules.[8,9] These aspects are not only theoretical considerations but are also critical to practical knowledge about metallic clusters in various applications, such as catalysis,[10–12] biocatalysis,[13] sensors[14] and biosensors,[15] and biological processes,[16] among many others.

In 2018, a new type of chemical bond, the metavalent bond, appeared in chemical literature,[17,18] describing many cases of multicentric electron-deficient (featuring less than two shared electrons), soft and longer bonds, distinct from single covalent, ionic, and metallics bonds: the metavalent bond. This new bond type is a good candidate to be considered for small metallic clusters in various environments, including homonuclear metallic dimers in peptides, proteins, and nucleic acid. With respect to metal-biomacromolecule bonding, the best description that can be given is the charge-shift bond,[19] a chemical bond resulting from the resonance of several ionic structures of species in question. Charge-shift bonding comprises a few non-typical covalent bonds, namely dative, coordinative, and hypervalent bonds.[19]

This study investigates homonuclear metal dimers within biomacromolecules, exploring their presence throughout the periodic table through structural database formation, and rationalising dimer bonds in comparison with the respective metallic bonds. The basic hypothesis is that the dimer bonds do not conform to any classical bond type but are instead metavalent, borderline cases between metavalent/covalent, or metavalent/metallic bonds. To further develop this hypothesis, the study additionally focused on two metals. Firstly, a structural database for all silver clusters was created, and the data were analysed to show that the metallic character of cluster bonds appears in larger clusters. Secondly, a structural database for potassium clusters was generated, and the data were analysed to show

* Dr. Rudolf Kiralj, PhD
Email: rkiralj@vub.hr

that electron donation by donor ligands causes changes in partial atomic charges and atomic radii of potassium atoms. These phenomena, observed for selected potassium dimers, do not agree well with classical bond types, but point to the metavalent bond or its borderline cases. Several structural parameters were defined, calculated, and analysed using statistical methods.

2 Methods

2.1 All metal dimers in biomacromolecules: Initial database creation

A database of homonuclear metal (M) dimers in biomacromolecules was constructed by searching for well-defined M–M dimers in crystal structures resolved by diffraction methods (X-ray, neutron, and synchrotron diffraction), and with known space groups in the *Protein Data Bank* (PDB).[20]

The following criteria were applied to select each dimer: 1) Dimer atoms were not part of a larger cluster of the same element through normal or weak bonds; 2) The sum of the occupancies of dimer atoms was greater than 1.00; 3) Dimers with weak metal-metal bonds (so-called metallophilic interactions) were included only if the interatomic distance fell within a specific range determined for each element (d_{max} range for element with atomic number Z, Table 1); 4) Dimers with too short, *i.e.*, multiple M–M bonds, were not included.

Biomacromolecular crystal structures from the PDB database were analysed using molecular graphics software

Table 1 – Selection criteria for M–M bonds (normal and weak) in metallic dimers identified within biomacromolecular structures in crystals, and the corresponding absolute frequencies

Tablica 1 – Kriteriji za probir veza M–M (normalnih i slabih) u metalnim dimerima koji su pronađeni u biomakromolekulskim strukturama u kristalima i pripadne apsolutne frekvencije

M	Z	d_{max}/Å	$2r_{vdW}$/Å	d_0/Å	$2r_{cov1}$/Å	$2r_{cov2}$/Å	$2r_{cov3}$/Å	λ_0	v	F
Li	3	3.0–3.2	4.24	3.039	2.66	2.48	–	0.250	2	1
Na	11	3.7–4.2	5.00	3.716	3.20	3.10	–	0.250	2	19
Mg	12	3.2–3.4	5.02	3.197	2.78	2.64	2.54	0.500	3	47
K	19	4.2–4.8	5.46	4.544	3.92	3.86	–	0.250	2	17
Ca	20	3.8–4.3	5.24	3.947	3.42	2.94	2.66	0.333	3	9
V	23	2.9–3.1	4.84	2.622	2.68	2.24	2.12	1.250	3	3
Mn	25	2.9–3.1	4.90	2.731	2.38	2.10	2.06	0.500	2	20
Fe	26	2.9–3.1	4.88	2.482	2.32	2.18	2.04	0.750	3	211
Co	27	2.9–3.1	4.80	2.506	2.22	2.06	1.92	0.500	2	2
Ni	28	3.2–3.4	4.80	2.492	2.20	2.02	2.02	0.333	3	1
Cu	29	3.1–3.3	4.76	2.556	2.40	2.30	2.24	0.333	2	56
Zn	30	3.1–3.3	4.78	2.665	2.40	2.36	–	0.500	2	34
Ga	31	3.0–3.2	4.64	2.442	2.48	2.42	2.34	0.800	2	1
Rb	37	4.5–5.3	6.42	4.950	4.20	4.04	–	0.250	2	4
Sr	38	3.9–4.7	5.68	4.303	3.70	3.14	2.78	0.333	3	18
Mo	42	3.1–3.5	4.90	2.725	2.76	2.42	2.26	0.750	3	2
Ru	44	2.9–3.1	4.92	2.650	2.50	2.28	2.06	0.750	2	1
Rh	45	2.9–3.1	4.88	2.690	2.50	2.20	2.12	0.500	2	14
Pd	46	3.2–3.5	4.30	2.751	2.40	2.34	2.24	0.333	2	2
Ag	47	3.4–3.7	5.06	2.889	2.78	2.74	2.56	0.167	2	31
Cd	48	3.6–3.9	4.58	2.979	2.88	2.72	–	0.500	2	8
Cs	55	5.3–6.1	6.96	5.309	4.64	4.18	–	0.250	2	24
Ba	56	4.5–5.4	6.06	4.377	3.92	3.22	2.98	0.500	3	23
La	57	3.9–4.3	4.96	3.739	3.60	2.78	2.78	0.750	2	1
Eu	63	4.0–4.4	5.64	3.989	3.36	2.68	–	0.750	2	1
Dy	66	4.0–4.4	5.62	3.503	3.34	2.66	–	0.750	2	2
Ho	67	4.0–4.4	5.66	3.486	3.32	2.66	–	0.750	2	1
Au	79	3.2–3.6	4.90	2.884	2.48	2.46	2.42	0.500	2	1
Hg	80	3.4–4.0	4.94	3.005	2.66	2.64	–	0.500	2	4
Tl	81	3.5–4.0	5.20	3.408	3.00	2.88	2.84	0.750	3	5
Pb	82	3.5–4.0	5.08	3.500	2.88	2.74	2.70	0.333	2	2

ViewerLite[21] and *Mercury*.[22] Biomacromolecules included peptides, proteins, DNAs, RNAs, DNA-RNA hybrids, and complexes of two or three types of these compounds. Dimers appeared in three forms: 1) Two metal ions forming a dimer in a biomacromolecule; 2) Two metal atoms as part of a cofactor within a biomacromolecule; 3) Two metal atoms within an organic or inorganic species bound to a macromolecule.

2.2 All metal dimers in biomacromolecules: Additional calculations and data analysis

The following structural parameters for metals were used from *Webelements.com*[23] (Table 1): r_{vdW} – van der Waals radius, d_0 – bond length in pure crystalline metal, r_{cov1} – molecular single bond covalent radius, r_{cov2} – molecular double bond covalent radius, and r_{cov3} – molecular triple bond covalent radius (when available). Combining these data with the measured bond lengths *d* for dimers from the PDB database, some new bond descriptors were defined. The relative bond length of an M–M dimer, δ, was defined using Eq. (1).

$$\delta = \frac{d}{2r_{vdW}} \tag{1}$$

The relative M–M bond length of the corresponding pure crystalline metal, δ_0, was calculated according to Eq. (2).

$$\delta_0 = \frac{d_0}{2r_{vdW}} \tag{2}$$

The difference of these two relative bond lengths, ε, was given by Eq. (3).

$$\varepsilon = \delta - \delta_0 \tag{3}$$

The observed bond order λ_0 of a pure crystalline metal (Table 1) was simply determined as the number of electrons divided by the number of metallic bonds (understood as individual metal-metal close contacts) in a unit cell. Knowing the packing type of metals (from *Webelements.com*[23]), it was easy to count the number of bonds and the number of atoms belonging to a unit cell. The number of electrons was calculated as the number of atoms multiplied by the number of lost electrons *per* atom (from the most common oxidation state of the metal). The only non-trivial case was that of gallium, with a complicated crystal structure (COD ID 9008085 from the *Crystallography Open Database*),[24] which had to be carefully analysed using *ViewerLite* software.[21]

Bond length – bond order polynomial regression equations for metals from Table 1 were determined using available data: interatomic distances $2r_{vdW}$, d_s, $2r_{cov1}$, $2r_{cov2}$, $2r_{cov3}$ and bond orders 0, λ_0, 1, 2, 3, respectively. The regression equations were obtained using online software *Polynomial Regression Data Fit*,[25] and the maximum degree of polynomials ν was 2 or 3 (Table 1). For dimers from the PDB database, the bond order λ was determined from the corresponding regression equation in the reversed sense: bond lengths were calculated for several bond orders until the bond length obtained was the closest to the experimental *d* value (difference below 0.001 Å). The same reverse procedure was applied to determine the calculated values λ_c from d_0 for pure metals. The all-metals database was aimed to contain bond orders roughly around 1 and between 0 and 1, and thus, all dimers with obtained $\lambda > 1.3$ were not included. The number of dimers (absolute frequency *F*, Table 1) was finally determined for each metallic element.

Finally, the two calculated bond orders, λ and λ_c, were compared in terms of their difference μ, as defined by Eq. (4).

$$\mu = \lambda - \lambda_c \tag{4}$$

Calculated bond orders were preferred over observed values for pure metals due to the overprediction tendency of bond length – bond order relationships for most metals. The final database for all metal dimers contained *Z* and dimer descriptors *d*, δ, ε and μ.

Bond descriptors, δ, ε and μ, were further analysed in terms of their frequency distribution, in order to assess the degree of similarity between dimer bonds and pure metallic bonds. Empirical distributions were analysed and tested for normality, and corresponding theoretical distribution curves were generated using the statistics programme *JASP*.[26] Additional analysis of the distributions by metallic elements were performed using scatterplots of δ, ε, and μ *versus Z* with the chemometrics package *Pirouette*.[27]

2.3 Bonds per atom – bond length deviation relationship for silver: Database creation

Among all the metals found in dimer form within biomacromolecular structures, silver was selected to establish an example of bonds *per* atom (β) – bond length deviation (Δ) relationship to be extended to all the other metals. The bonds *per* atom, β, is the average number of Ag–Ag bonds *per* Ag atom, equivalent to half the average bonding coordination sphere of Ag atoms around an Ag atom. This quantity is better than the number of Ag atoms, volume, surface or some other quantity accounting for size of Ag clusters, nanostructures, or more complex structures. The bond length deviation is the absolute difference between the clusters' average Ag–Ag bond length and the standard Ag–Ag bond length in bulk metal at room temperature and normal pressure (2.889 Å).[28–30] As β values increase, the size of Ag structures also increases in such a way that an Ag atom has more and more neighbouring Ag atoms. This enhances valence electron delocalisation, resulting in Ag–Ag bonds that become more metallic and more similar to those in bulk silver.

A database for Ag–Ag bonds was generated from four types of sources. Three-dimensional structures containing Ag–Ag bonds were retrieved from structural databases, including the *Protein Data Bank*,[20] the *Cambridge Structural Database*,[31] the *Inorganic Crystal Structure Database*,[31] the *Crystallography Open Database*,[24] and the *American Mineralogist Crystal Structure Database*,[32] or from supplementary materials to published articles. In other case, supplemen-

tary materials served to generate three-dimensional coordinate files. In all cases, three-dimensional structures from the coordinate files were carefully examined using molecular graphics software *ViewerLite*[21] and *Mercury*.[22] Average interatomic distance (d_{av}) and bonds *per* atom (β) were determined, with deviation (Δ) calculated according to its definition. Both d_{av} and β were taken from numerous articles or supplementary materials as direct data, and as data estimated from available information in textual, numerical, or pictorial form. Literature sources were combined whenever necessary.

Silver nanostructures represent a unique category of pure silver structures, where a substantial fraction of Ag atoms is located at the surface, resulting in a half-filled coordination sphere with neighbouring silver atoms. For such nanostructures, bonds *per* atom, β, was calculated using formulas developed in this study, where the final β value was defined by Eq. (5):

$$\beta = 3(2-u) \tag{5}$$

The factor *u* was calculated differently for nanostructures of distinct shapes. For spherical nanoparticles with radius ρ in Å units, *u* was defined by Eq. (6).

$$u = 8.87274\left(\rho / \text{Å}\right) \tag{6}$$

For thin films with thickness *D* in Å units, *u* was calculated using Eq. (7).

$$u = 2.04326\text{Å}\left[1+\left(D / \text{Å}\right)^{-7}\right] / D \tag{7}$$

For cylinders with radius ρ and height *h* in Å units, *u* was obtained using Eq. (8).

$$u = 5.89588\frac{(\rho+h)\text{Å}}{\rho h} \tag{8}$$

The majority of structures contained normal Ag–Ag bonds. In some cases, for illustrative purposes, and to incorporate some structures with β values between 0 (Ag...Ag contact) and 0.5 (Ag_2 dimer), weaker Ag–Ag bonds, interactions, and contacts were also included (Table 2). The true average bond length or interatomic distance, as well as the true β value, had to be calculated using an appropriate weighting scheme (Table 2).

In such cases, the true number of bonds n_b was calculated using Eq. (9):

$$n_b = \sum_i^n w_i \tag{9}$$

where *n* is the total number of all bonds, interactions, and contacts, and w_i is the appropriate weight from Table 2 for the *i*-th bond, interaction or contact. The β value was obtained from a simple Eq. (10).

Table 2 – Criteria for classification of Ag–Ag bonds, interactions, and contacts according to metal-metal distance, along with corresponding weighting factors

Tablica 2 – Kriteriji za klasifikaciju veza, interakcija i kontakata Ag–Ag prema udaljenosti metal-metal, s pripadnim faktorima uteženja

Bond/ interaction	Normal bond	Weak bond	Very weak bond	Argentophilic interaction	Contact
d(Ag...Ag)/Å	≤ 3.4	3.4–3.7	3.7–4.0	4.0–4.3	≥ 4.3
w	1	0.5	0.25	0.125	0

$$\beta = n_b / 2 \tag{10}$$

The average bond length d_{av} was calculated using Eq. (11):

$$d_{av} = \sum_i^n w_i d_i / n_b \tag{11}$$

where d_i is the interatomic distance of the *i*-th bond, interaction or contact. When only one contact was reported, the values were $\beta = 0$ and $d_{av} = d$.

2.4 Bonds *per* atom – bond length deviation relationship for silver: Data analysis

Graphical analysis of bonds *per* atom – bond length deviation scatterplots was performed using programming, numerical computing, and graphics software *Scilab*[33] for various types of silver structures (biomacromolecular silver in crystals, elementary silver, organic and organometallic, inorganic and intermetallic silver, and others). Silver clusters in biomacromolecular structures in crystals and other structure types of silver exhibited a consistent decrease in maximum Δ values as β increased. This relationship was modelled non-linearly and further tested for statistical significance of the obtained equations through the online curve fitting software *MyCurveFit*.[34]

2.5 Charge-radius relationship for potassium: Database creation and data analysis

Potassium was selected among many metals found in dimer form within biomacromolecules, to illustrate an example of a charge (*Q*) – radius (*R*) relationship for these metals. It is assumed that the partial atomic charges of metal atoms in these dimers correspond to a certain electron content that defines the size of the two metal atoms, and consequently, the bond length of the dimer. However, the dimer's electron content is strongly influenced by the ligand atoms that donate partial negative charge (electrons) to the dimer. These ligand atoms, when bound to the dimer, "sense" the dimer, and therefore, the geometrical arrangement of the ligands will always adapt to the dimer. From this arrangement, valuable geometric data can be extracted to estimate the radii and even the charges of the metal atoms.

To simplify, the average features of dimer atoms were calculated in this study. All the methods developed here are qualitative but sufficiently reliable, as they are based on a large number of data. A quantitative approach would require highly sophisticated quantum-chemical methods focused on specific classes of compounds containing K–K dimers.

A database for potassium charge and radius values was constructed from the literature in various ways. Whenever possible, both charge and radius values were obtained from a single literature source (articles, supplementary materials, online sources) as direct data, or as data estimated from available textual, numerical, or pictorial information. In cases where only one value was available, either charge or radius, the literature sources were combined or the other value was sourced from another reliable reference.

Several times, molecular structures of potassium clusters or crystal structures containing potassium were taken from the *Protein Data Bank*,[20] the *Cambridge Structural Database*,[31] and the *Inorganic Crystal Structure Database*,[31] or from supplementary materials in published articles. Where necessary, supplementary materials were used to generate three-dimensional coordinate files. All three-dimensional structures were then analysed using molecular graphics software *ViewerLite*[21] and Mercury.[22] Potassium binding radii were measured as half of the K–K bond length. When isolated K atoms were present in crystal structures, half of a close bond length E–E (E is any other chemical element) was used as covalent radius of E, and this value was then subtracted from the bond length of a neighbouring K–E bond. The additivity scheme of binding radii to yield bond lengths was suitable approximation for the purposes of this study. In cases where the *Q* value was missing, a formal charge or a charge from a closely similar structure was assigned when appropriate. The potassium charge - radius database comprised all potassium forms (metallic, cluster, nanoparticle, gas phase, oxidised in compounds), both from experimental and theoretical investigations. The potassium charge-radius relationship was examined in two forms: 1) as a linear relationship, established *via* linear regression at an 0.05 significance level using online software *Polynomial Regression Data Fit*[25] and *Linear Correlation and Regression (VassarStats)*[35]; 2) as a non-linear, sigmoid relationship, not based on regression analysis. The final charge - radius scatterplot with the line and curve was generated using *Scilab*.[33]

2.6 Molecular graphics as a structural tool in measuring molecular geometry

Four examples of macromolecules containing potassium were selected to test the charge-radius relationship and demonstrate its applicability: a protein, nucleic acids (DNA and RNA), and a protein-nucleic acid complex. *ViewerLite*[21] and *Mercury*[22] were used to identify, extract, and analyse K–K dimers from the selected biomacromolecular structures, which were already included in the all metal dimers database. Final identification of binding coordination spheres (coordination number 6 or 7 around each K atom, excluding the K–K bond), measurement of contact distances, and visual representations of the dimer coordination were completed using *ViewerLite*.[21]

Interatomic distances were identified based on the following criteria: For K–O bond length, the upper limit of 3.3 Å was chosen, a midpoint between the limits 3.1 Å proposed by *Gagné et al*.[36] and 3.5 Å proposed by *Nelyubina et al*.[37] For K–N bond length, an upper limit of 3.1 Å was set, slightly higher than the 2.9 Å limit suggested by *Kobasi et al*.[38] In the case of K–O(π), K–N(π) and K–C(π) bonds, the upper limit of 3.7 Å for metal – π-system distance from *Berionni et al*.[39] was used. Covalent radii of O and N were assumed not to vary significantly in covalent compounds; therefore, medium values[23] of 0.66 Å and 0.71 Å, respectively, were used. For the purpose of measuring K–X(π) interaction distances and K–X contact distances, the values of van der Waals radii[23] 1.50 Å, 1.66 Å and 1.77 Å for O, N, and C, respectively, were used. The upper limit for contact (non-bonding) interactions was set at 4.3 Å.

2.7 Estimation of radii and charge values of potassium from structural parameters

The following methods were developed to obtain structural parameters for K–K dimers. The ligand-based method 1 involved the following steps: 1) Measurement of K–X (X = O, N) and K–X(π) (X = O, N, C) distances; 2) Conversion of the distances into potassium bonding radius *R* values by subtracting the covalent or van der Waals radii of X from the distances; 3) Averaging the obtained *R* values; 4) Calculation of charge *Q* of potassium using the linear regression *Q*–*R* relationship in the inverse form of the equation; 5) Calculation of the bond order *B via* Eq. (12).

$$B = 1 - Q \tag{12}$$

The ligand-based method 2 followed the same steps, except for step 4), where charge *Q* of potassium was determined using the non-linear *Q*–*R* relationship in the inverse sense (*R* was iteratively calculated for many *Q* values until the closest *R* was achieved, below the difference of 0.001 Å). For incomplete K–K dimer bonding coordination spheres, a careful visual inspection was made, and additional water molecules with K–O distance 2.80 Å were included in calculating the average binding radius *R* of potassium.

The dimer-based methods 1 and 2 were based on the measured *R* value as $R = D_d/2$, where D_d was the K–K bond length. Using *R, Q* was then calculated through either the linear (method 1) or non-linear *Q*–*R* relationship (method 2), and finally, *B* was determined from *Q* using Eq. (12). Dimer-based method 3 used the D_d value for $R = D_d/2$ and to calculate *Q*. A previously derived bond order – bond length relationship for potassium for the all metal dimers database, defined by Eq. (13), was used in the inverse sense in the dimer-based method 3.

$$D_d \,/\, \text{Å} = 5.3022 - 2.2650B + 0.77758B^2 \tag{13}$$

Finally, for non-bonding contacts, only one method was used. From the measured interatomic distances K ... X, the corresponding van der Waal radii of X were subtracted, and the resulting values of non-bonding radii R_{nb} were averaged.

2.8 Placing the estimated charges of potassium in biomacromolecules into the space of metavalent bonding

The position of metavalent bonds between single covalent and metallic bonds, and near ionic bonds, can be effectively visualised through a scatterplot depicting the transferred electrons (*T*) – shared electrons (*S*) relationship.[42] Here, *T* is the amount of electrons transferred from one to another atom in a chemical bond, while *S* quantifies the electrons shared by the two atoms in the bond. A small database of *S* and *T* values for pure substances was constructed, with *S* defined as "uncorrected" (not divided by oxidation states).

Furthermore, *S* and *T* values for K–K dimers in macromolecules were determined from estimated average charges (Section 2.6), using a simple scheme $T = 0$ (dimer atoms of equal charge) and $S = 2 - 2Q$. However, a more complex model was also applied: the ligand-based methods 1 and 2 were reused to determine charges of both dimer atoms separately (averaging particular *R* values for each atom, and then calculating the *Q* values). Using this approach, *T* was calculated as the absolute difference between the two charges, and *S* was equal to the difference between 2 and the sum of the charges. The final *S*–*T* scatterplot was constructed using *Scilab*.[33]

3 Results and discussion

3.1 All metal dimers in biomacromolecules

A new database containing 565 entries, including *Z* values, bond lengths, and bond orders with their derived values δ, ε, and μ (using parameters from Table 1) was compiled for M_2 homonuclear metallic dimers in crystal structures of biomacromolecules. In total, 31 metals were found to form such dimers, as presented in Table 1. These metals span various parts of the periodic table: *s*-block metals (Li, Na, Mg, K, Ca, Rb. Sr, Cs and Ba), transition metals (V, Mn, Fe, Co, Ni, Cu, Zn, Mo, Ru, Rh, Pd, Ag, Cd, Au and Hg), *p*-block metals (Ga, Tl and Pb), and lanthanides (La, Eu, Dy and Ho). This observation indicates the universality of homonuclear M_2 dimers in biomacromolecules, highlighting that any metal can form M_2 dimers and retain this form in crystals of biomacromolecules. The extensive search for M_2 dimers within the PDB database revealed two principal ways of formation of these dimers: 1) From metallic ions, which bind next to each other, often connected by bridging ligands; 2) As part of natural or artificial species (co-factors, inhibitors, substrates, other reactive agents), which covalently or non-covalently bind to a macromolecule.

However, the 31 metals significantly differ in terms of absolute frequencies of the M_2 dimers found (Table 1). The most abundant is the Fe_2 dimer, mainly present in the Fe_2S_2 cluster in proteins. This cluster was found in more than 1250 crystal structures within the PDB database, therefore, a selection had to be applied to avoid iron data overload. For all other metals, no selection was made; instead, all available data were used included in the new database. Other more frequent metals ($F > 10$) included Na, Mg, K, Mn, Cu, Zn, Sr, Rh, Ag, Cs, and Ba. Some metals, such as Li, Ni, Ga, Ru, La, Eu, Ho, and Au were represented by unique dimers.

More insight into the database structure could be gained from analysing the empirical distribution (Table 3 and Fig. 1), and the theoretical distribution (Fig. 1) of the dimensionless variable δ, the M–M bond length relative to twice the van der Waals radius (Eq. (1)). The data were centred at the mean of 0.61, with a moderate range of 0.42 and a coefficient of variation of 0.14. The empirical distribution was non-normal, as evidenced by a significant difference between the mode and the mean/median, pronounced asymmetry – positive skewness (in bold), and a statistically significant Shapiro-Wilk non-zero statistic (in bold). The theoretical distribution (Fig. 1) appeared at least bimodal, with peaks at δ values of 0.55 and 0.63, as well as a pronounced right tail.

Examining the distribution curve and the rug marks, potential peaks were identified at 0.73, 0.78, and 0.83 within the tail, suggesting that the distribution could be considered a

Table 3 – Basic statistics for the distribution of parameters δ, ε, and μ
Tablica 3 – Osnovna statistika raspodjele parametara δ, ε i μ

Descriptive statistics parameter	δ	ε	μ
Mean (Standard error of mean)	0.620(4)	**0.034(2)**	**−0.076(8)**
Median	0.609	**0.042**	**−0.120**
Mode	0.523	**0.014**	**−0.126**
Minimum, Maximum	0.464, 0.882	−0.151, 0.205	−0.513, 0.647
Range	0.418	0.356	1.160
Standard deviation	0.088	0.058	0.184
Coefficient of variation	0.142	**1.698**	**−2.411**
Skewness (Standard error of skewness)	**0.903(103)**	**−0.326(103)**	**0.840(103)**
Kurtosis (Standard error of kurtosis)	0.153(205)	0.341(205)	**1.337(205)**
Shapiro-Wilk test statistic	**0.917**	**0.985**	**0.954**
Shapiro-Wilk probability	**< 0.001**	**< 0.001**	**< 0.001**

combination of five Gaussian distributions. This complex distribution cannot be readily explained by the positions of the metals in the periodic table. The right tail beyond $\delta = 0.7$ consisted mainly of M_2 dimers of the largest atoms (*s*-block metals). The left tail primarily corresponded to some transition metals. However, all other parts of the curve presented mixtures of various metals. More frequent metals appeared in various parts of the curve; for example Mg, Fe, and Ag were present throughout.

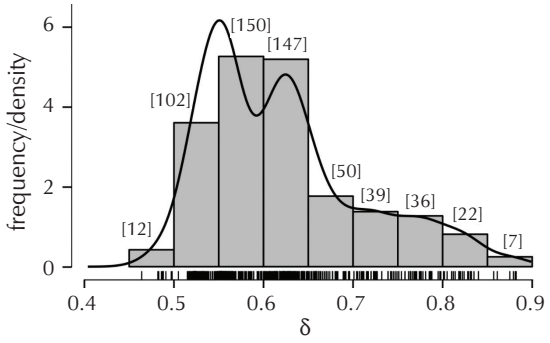

Fig. 1 – Distribution of the variable δ for all metal dimers in crystal structures of biomacromolecules: Histogram with absolute frequency values displayed above each column and rug marks at the bottom, overlaid with the corresponding density curve.

Slika 1 – Raspodjela varijable δ za dimere svih metala u kristalnim strukturama biomakromolekula: histogram s vrijednostima apsolutnih frekvencija (na vrhu svakog stupca) i s crtičastim oznakama na dnu, preklopljen s pripadnom krivuljom gustoće.

Values of d_{max} in Table 1 have already highlighted the flexibility of metals in forming dimers: M–M bonds can range from normal-length or weaker bonds, while dimers involving very weak bonds (*e.g.*, metallophilic interactions) were excluded from this study. The statistical analysis of the δ-values alone does not provide insight into the nature of the M–M bonds — whether they are metallic or of another type.

To address this, the variables ε and μ, representing the bond length (Eq. (3)) and bond order (Eq. (4)) relative to the pure metal, respectively, were calculated. Their distribution analysis (Table 3, Figs. 2 and 3) revealed significant deviations from metallic bonds in several statistical parameters (bolded in the table). In an ideal scenario, where all M–M dimer bonds in biomacromolecules are metallic exactly as in pure metals, the histograms would be positioned at zero mean, median, and mode, with minimal dispersion, and the distributions would be normal. The standard error of the mean for ε and μ was small, indicating that their means could not be considered zero. The dispersion in the histograms was obvious. The values of the coefficient of variation were extremely positive (1.70 for ε) and negative (−2.41 for μ). This confirmed that most metal dimers in biomacromolecules significantly deviate from M–M pairs in pure metals. Moreover, both distributions were non-normal: ε showed a smaller positive skewness, whereas μ exhibited a more pronounced positive skewness. The kurtosis was significantly below 3, indicating platykurtic distributions, *i.e.,* having shorter tails than the normal distribution. Finally, the Shapiro-Wilk normality test confirmed that the distributions were non-normal, as the test statistics were significantly different from zero in both cases.

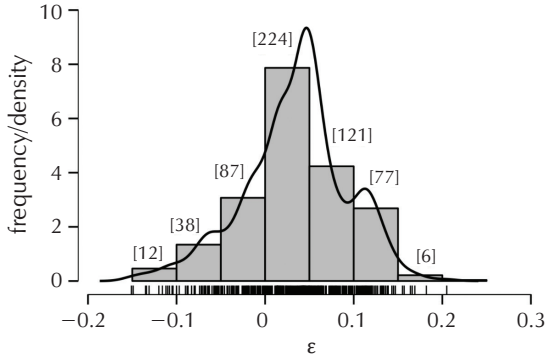

Fig. 2 – Distribution of the variable ε for all metal dimers in crystal structures of biomacromolecules: Histogram with absolute frequency values (displayed above each column) and rug marks at the bottom, overlaid with the corresponding density curve.

Slika 2 – Raspodjela varijable ε za dimere svih metala u kristalnim strukturama biomakromolekula: histogram s vrijednostima apsolutnih frekvencija (na vrhu svakog stupca) i s crtičastim oznakama na dnu, preklopljen s pripadnom krivuljom gustoće.

Examining the theoretical distributions for ε (Fig. 2) and μ (Fig. 3), the multimodal character of the curves became apparent, suggesting they were composed of several normal distributions. The curve for ε exhibited three modes at values of ε equal to −0.06, 0.05, and 0.12. Addition-

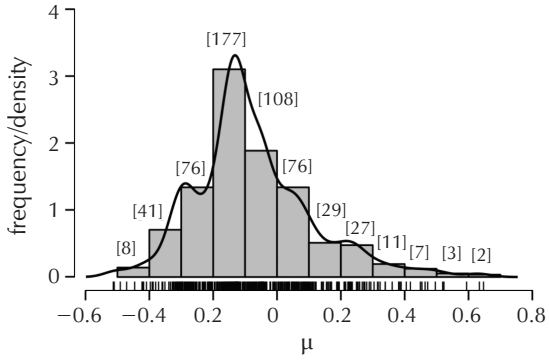

Fig. 3 – Distribution of the variable μ for all metal dimers in crystal structures of biomacromolecules: Histogram with absolute frequency values (above each column) and rug marks at the bottom, overlaid with the corresponding density curve.

Slika 3 – Raspodjela varijable μ za dimere svih metala u kristalnim strukturama biomakromolekula: histogram s vrijednostima apsolutnih frekvencija (na vrhu svakog stupca) i s crtičastim oznakama na dnu, preklopljen s pripadnom krivuljom gustoće.

ally, potential modes appeared at −0.03 and 0.03 units of ε. This suggested that the curve may be a superimposition of five Gaussian distributions. A very similar pattern was observed in the curve for μ, which had four visible modes at values −0.29, 0.13, 0.05, and 0.23, with a potential mode at −0.06 units of μ. Again there were five Gaussian distributions, and this was also the case with the δ curve.

Analysing the distributions by metal revealed similar trends to those observed for the distribution of δ. Metals were mixed across all parts of the curves, with no metal preference for any particular part. Many metals, such as Na, Fe, and Ba, appeared in most parts of the two curves. This diversity of M–M dimers found in biomacromolecules suggested the existence of dimer bonds with large variations in lengths (defined by d_{max} values in Table 1) and bond orders. Most bond orders λ were smaller than 1, similar to the values of λ_0 for pure metals (Table 1).

Considering the distributions of ε and μ, it could be concluded that M–M bonds in homonuclear metallic dimers within biomacromolecules cannot be strictly characterised as typical metallic, covalent, or ionic bonds. Biomacromolecular structures contain various ligands, which contribute to the pronounced variability in M–M bond parameters: these include peptide bonds, carbonyl, hydroxyl, amino, carboxylate, phosphate, sulfhydryl, and other groups as ligands, π-system ligands, water and other solvent molecules, halides, groups of small inorganic and organic molecules, and even other metallic cations, among others. All these findings suggested that the M–M bonds in question were metavalent bonds, borderline metavalent/covalent, or even metavalent/metallic bonds. During the search for M_2 dimers in the PDB database, dimers with very short metal-metal bonds were identified for various metals. However, these were excluded from the analysis because they represented multiple bonds, which form through mechanisms different from those of the studied bonds, pure metallic bonds, and single covalent bonds.

3.2 Bonds *per* atom – bond length deviation relationship for silver

A database containing 761 entries of bonds *per* atom (β) and bond length deviation (Δ) values for silver clusters, was created and organised into nine modules (Table 4). Silver is a very versatile metal, appearing in various types of compounds and in elementary forms such as bulk, clusters, and nanostructures. It has been studied in the gas, liquid, and solid phases. The modular organisation of the database highlighted silver's versatility and revealed sharper trends than when considering the database as a whole. Table 4 presents the basic statistics of the database and its modules: N_{tot} – total number of database entries; N_w – number of entries for structures containing weak and very weak Ag–Ag bonds, argentophilic interactions and contacts; N – number of entries for structures with normal Ag–Ag bonds; β_{min} and β_{max} – minimum and maximum values of β, respectively; Δ_{min} and Δ_{max} – minimum and maximum values of Δ, respectively. These β and Δ values are reported for normal Ag–Ag bonds, as these bonds are the primary focus of the analysis of dimers and larger clusters.

Inspection of Table 4 revealed several noteworthy conclusions. Bulk silver in its crystalline state consisted of Ag atoms with a β value equal to 6 (half of its coordination number 12). Silver nanostructures varied considerably in size and shape, so that β ranged from 2.6 to nearly 6. All other modules encompassed structures ranging from Ag dimers to three-dimensional arrangements of Ag atoms, similar to the structure of bulk silver. Only biomacromolecules in solution displayed a narrow range of β values for various Ag_3 clusters, due to the small number of available structures. Regarding Δ, the minimum values were not informative, but the maximum values indeed showed the expected tendency. Pure silver forms (bulk and nanostructures) exhibited the smallest Δ_{max} values (0.1–0.2 Å), and structures in other modules showed significant values (0.4–0.6 Å). This trend can be understood as a consequence of three factors: 1) The influence of chemical bonding with non-silver atoms in the structure; 2) The effect of physical conditions (melting, freezing, high pressure, etc.); and 3) The size of Ag structures.

Table 4 – Basic statistics for the silver database and its modules
Tablica 4 – Osnovna statistika baze podataka za srebro s njezinim modulima

Database modules	N_{tot}	N_w	N	β_{min}/Å	β_{max}/Å	Δ_{min}/Å	Δ_{max}/Å
Biomacromolecules (crystal)	72	8	64	0.500	2.889	0.014	0.562
Biomacromolecules (solution)	51	40	11	1.000	1.286	0.129	0.438
Organics & organometallics (crystal)	116	20	96	0.500	4.765	0.002	0.556
Silver clusters (gas phase)	143	0	143	0.500	4.043	0.005	0.470
Silver clusters in processes/reactions	98	2	96	0.500	4.368	0.002	0.377
Melt, frozen & other silver structures	86	0	86	0.500	6.000	0.000	0.449
Inorganics & intermetallics (crystal)	70	15	55	0.500	6.000	0.002	0.597
Elementary bulk silver	65	0	65	6.000	6.000	0.000	0.174
Silver nanostructures	60	0	60	2.500	5.997	0.000	0.107
Full database	761	85	676	0.500	6.000	0.000	0.597

When factors 1) and 2) are considered common contributors to Δ variation for a given β value, then factor 3) is to be studied for the entire range of β values. In other words, Δ can be considered as a function of β for a specific database module: the larger the Ag cluster, the more metallic are the Ag–Ag bonds. An example for this statement is presented in Fig. 4 for silver clusters in biomacromolecular structures in the crystalline state. Weak and very weak Ag–Ag bonds, as well as argentophillic interactions and Ag–Ag contacts, were included to encompass the full range of β values, from 0 to 0.5. The Δ_{max} values can be interpreted as the maximum variation of Δ at a given β value, justifying the use of some selected data points to construct a hyperbolic curve described by Eq. (14), where *j*, *k*, *l*, and *m* are non-integer coefficients.

$$\Delta / \text{Å} = j + \frac{k}{1 + \left(\frac{\beta}{m}\right)^{l}} \tag{14}$$

Although the curve is drawn through 9 data points and Fig. 4 represents 72 entries for biomacromolecules in crystal, the trends are apparent. Clusters larger than dimers (β > 0.5) exhibited decreasing Δ values, indicating that the average Ag–Ag bond became progressively more metallic. To the left of Ag_2 dimers (β < 0.5) are dimers and trimers with weak and very weak bonds, argentophillic interactions and Ag–Ag contacts. The Ag–Ag bond in normal Ag_2 dimers does not seem to be close to a pure metallic bond, but at the same time, it is much stronger than the mentioned weak bonds.

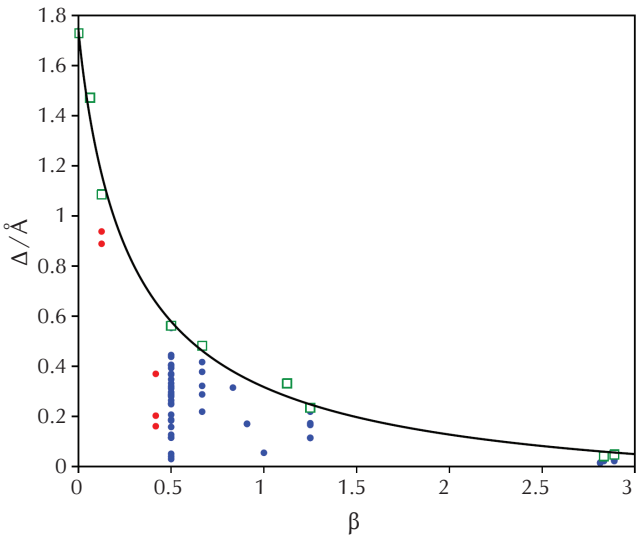

Fig. 4 – Bonds *per* atom (β) – bond length deviation (Δ) relationship for silver, based on 72 data points from a newly created database for silver clusters. Legend: Green squares – selected data points used to construct the curve representing the maximum variation in Δ; Blue dots – data points for normal Ag–Ag bonds (β ≥ 0.5) that were not included in curve construction; Red dots – data points for various weak Ag–Ag bonds, interactions, and contacts (β < 0.5) that were not included in curve construction.

Slika 4 – Odnos broja veza po atomu (β) i devijacije duljine veze (Δ) za srebro, baziran na 72 podatkovne točke iz novostvorene baze podataka za klastere srebra. Legenda: zeleni kvadratići – odabrane podatkovne točke kroz koje je povučena krivulja maksimalne varijacije u Δ; plave točke – podatkovne točke za normalne veze Ag–Ag (β ≥ 0.5) koje nisu rabljene u povlačenju krivulje; crvene točke – podatkovne točke za razne slabe veze, interakcije i kontakte Ag–Ag (β < 0.5) koje nisu rabljene u povlačenju krivulje.

A much larger number of data points would provide stronger evidence to illustrate the regularity of the bonds *per* atom – bond length deviation relationship. Comparisons of silver clusters in biomacromolecules in crystals with those in other database modules are shown in Figs. 5 and 6. This relationship cannot exist in elementary silver (Fig. 5), and is only faintly apparent in silver nanostructures (Fig. 6). Some other database modules, such as melted and frozen, and other silver structures (Fig. 5), silver clusters involved in processes/reactions, or found in the gas phase (Fig. 6), exhibited a general decrease in Δ with increasing β. However, these trends remained poorly defined due to insufficient data. Two additional trends emerged from the analysis: 1) The modules differed in the range of β values – some modules spanned the full range of β (up to six units), while others covered only a limited range; 2) The modules differed in the average position with respect to the horizontal axis - some modules were positioned closer, while others were farther from the β axis.

Fig. 7 builds upon Fig. 4 by extending the curvilinear relationship defined by Eq. (14) to all suitable modules. The equations were statistically significant at a significance level of $\alpha = 0.05$ ($r > 0.9860$, $p < 0.003$). The curve for biomacromolecules in crystals (blue) had a shape similar to the curves for organics and organometallics (green) and for inorganics and intermetallics (brown). These three curves shared nearly identical starting points at β = 0 and were mutually "parallel" at β > 1. The module for biomacromolecules in solution (red) exhibited distinct behaviour, starting differently and becoming parallel to the horizontal axis at β > 2, likely due to the limited number of available structures. Variations in bulk silver were even greater than the heights of the pink, blue, and green curves at β = 6, owing to the extreme physical conditions under which certain bulk silver structures were determined (*e.g.*, high pressure and temperature).

Each curve in Fig. 7 is a branch of a hyperbola. This branch can be divided into three parts, each of which may be qualitatively associated with different bond types. The first part of all four curves shows a rapid descent, resembling a straight line. This portion occurs at β < 0.4, and is associated with weak and very weak Ag–Ag bonds, argentophilic interactions, and Ag–Ag contacts. The next part of the curves shows a significant change in trend. It resembles a road bend and occurs around β = 0.5, extending to approximately β = 1.5 (pink curve) or to β = 3 (blue, green, and brown curves). This section can be related to metavalent bonds, borderline metavalent/covalent, or metavalent/metallic bonds in dimers, trimers, and other small clusters. The third part of the curves again appears as a straight line, gradually approaching the horizontal axis. This section is associated with larger silver clusters and smaller silver na-

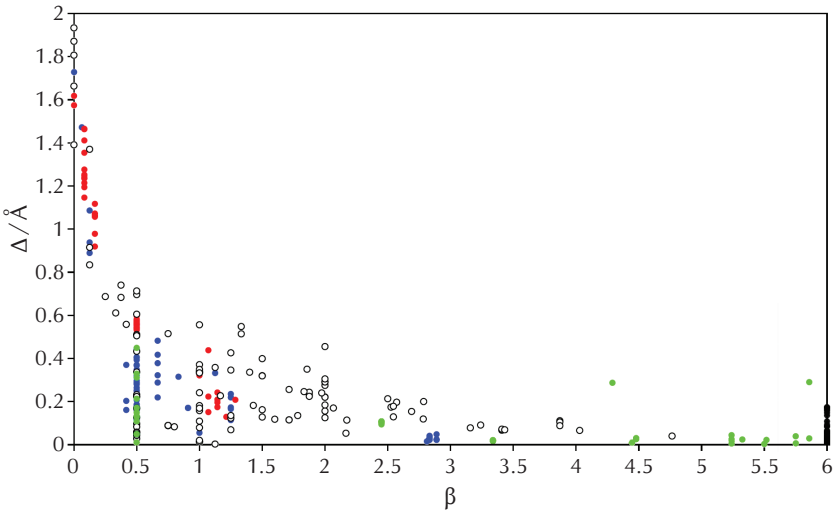

Fig. 5 – Bonds *per* atom (β) - bond length deviation (Δ) relationship for silver in structures from five modules of the newly created database, represented by coloured data points. Legend: blue – biomacromolecules in crystals; red – biomacromolecules in solution; white – organics and organometallics in crystals; green – melt and frozen and other silver structures; black – elementary bulk silver. A fairly consistent decrease in deviation Δ with increasing β is evident in most modules.

Slika 5 – Odnos broja veza po atomu (β) i devijacije duljine veze (Δ) za srebro u strukturama iz pet modula novostvorene baze podataka, predstavljen obojenim podatkovnim točkama. Legenda: plavo – biomakromolekule u kristalu; crveno – biomakromolekule u otopini; bijelo – organski i organometalni spojevi u kristalu; zeleno – rastaljene i smrznute te druge strukture srebra; crno – elementarno srebro. Pravilan pad devijacije Δ s porastom β prilično je dobro vidljiv za većinu modula.

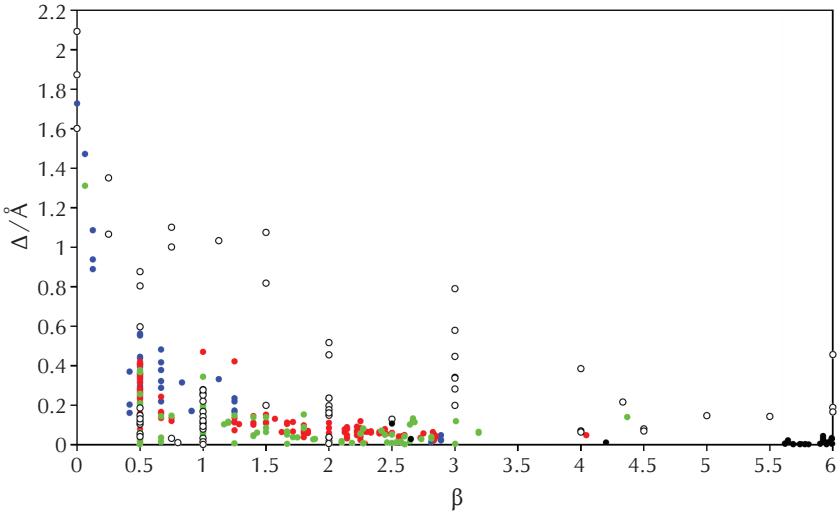

Fig. 6 – Bonds *per* atom (β) – bond length deviation (Δ) relationship for silver in structures from five modules of the newly created database, represented by coloured data points. Legend: blue – biomacromolecules in crystals; red – silver clusters in processes/reactions; white – inorganics and intermetallics in crystals; green – silver clusters in the gas phase; black – silver nanostructures. A fairly consistent decrease in deviation Δ with increasing β, is evident in most modules.

Slika 6 – Odnos broja veza po atomu (β) i devijacije duljine veze (Δ) za srebro u strukturama iz pet modula novostvorene baze podataka, predstavljen obojenim podatkovnim točkama. Legenda: plavo – biomakromolekule u kristalu; crveno – klasteri srebra u procesima/reakcijama; bijelo – anorganski i intermetalni spojevi u kristalu; zeleno – klasteri srebra u plinskoj fazi; crno – nanostrukture srebra. Pravilan pad devijacije Δ s porastom β prilično je dobro vidljiv za većinu modula.

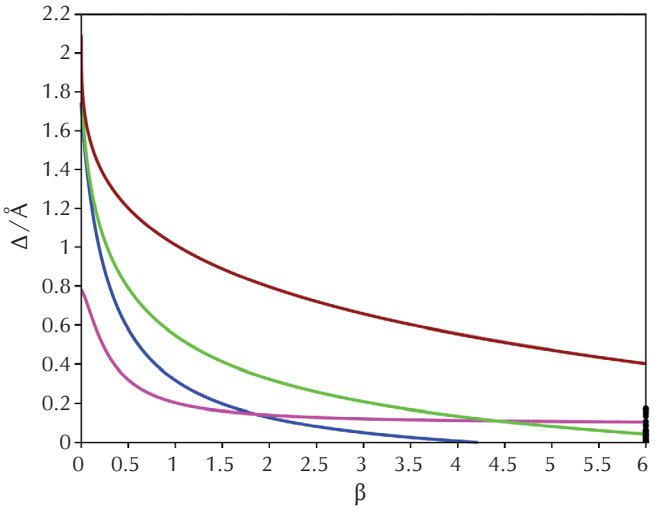

Fig. 7 – Bonds *per* atom (β) – bond length deviation (Δ) relationship for silver in structures from five modules of the newly created database, represented by coloured curves (curvilinear presentation of the maximum values of deviation Δ) and black dots. Legend: black – elementary bulk silver; blue – biomacromolecules in crystals; pink – biomacromolecules in solution; green – organics and organometallics in crystals; brown – inorganics and intermetallics in crystals.

Slika 7 – Odnos broja veza po atomu (β) i devijacije duljine veze (Δ) za srebro u strukturama iz pet modula novostvorene baze podataka, predstavljen obojenim krivuljama (krivolinijskom prezentacijom maksimalnih vrijednosti devijacije Δ) i crnim točkama. Legenda: crno – elementarno srebro; plavo – biomakromolekule u kristalu; ljubičasto – biomakromolekule u otopini; zeleno – organski i organometalni spojevi u kristalu; smeđe – anorganski i intermetalni spojevi u kristalu.

nostructures in compounds, where Ag–Ag bonds are metallic-like or metallic. The minimum value of β around 3 indicates that half of the coordination sphere around an Ag atom is occupied by other Ag atoms. For example, a silver cluster Ag_{16} bound to a DNA oligomer (PDB: 7XLW)[40] has a β value of 2.889, with minimum and maximum β values for atoms within the cluster being 1 and 4, respectively. This is an example of a cluster of 16 Ag atoms sharing valence electrons, allowing for electron delocalisation in a cycle of 16 atoms. As a result, the average Ag–Ag bond length is very similar to that of a metallic Ag–Ag bond. Another interesting observation from Fig. 7 is that the blue curve reached $\Delta = 0$ at $\beta = 4.213$, while the green and brown curves ended with $\Delta = 0.043$ Å and $\Delta = 0.401$ Å at $\beta = 6$, respectively. This suggested that the effect of ligand bonding on the Ag cluster was smallest in biomacromolecules, greater in organics and organometallics (where ligands are frequently delocalised π-systems), and greatest in inorganics and intermetallics (where ligands are frequently ions due to significant electronegativity differences).

3.3 Charge-radius relationship for potassium

A database containing 515 charge (*Q*) and radius (*R*) values for potassium was created. The charge-radius scatterplot is presented in Fig. 8. The general shape of the charge-radius relationship is sigmoidal. Some outliers with negative charges and radii between 1.5 and 2 Å are present. These correspond to dimers in solid Na-K alloys under extreme pressures, where potassium becomes electronegative with respect to Na.[41]

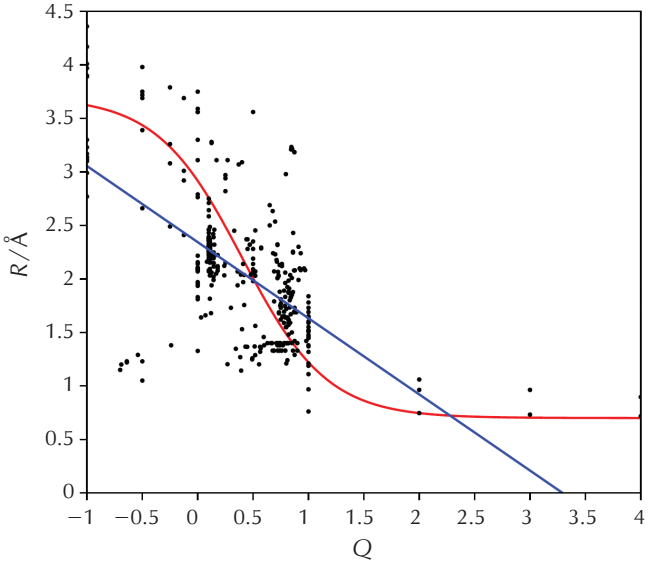

Fig. 8 – Partial atomic charge (*Q*) – radius (*R*) relationship for potassium, based on 515 data points from the newly created database. Legend: black dots – data points; blue line – linear regression line for charges ranging from 0 to 1; red curve – theoretical sigmoid curve covering the entire range of charge values.

Slika 8 – Odnos parcijalnog atomskog naboja (*Q*) i radijusa (*R*) za kalij, baziran na 515 podatkovnih točaka iz novostvorene baze podataka. Legenda: crno – podatkovne točke; plavo – pravac linearne regresije za naboje od 0 do 1; crveno – teorijska sigmoidna krivulja koja pokriva cijeli raspon vrijednosti naboja.

The sigmoidal shape of the charge-radius relationship is logical, as a potassium atom can gain or lose an electron, and even lose multiple electrons. When neutral K^0 is oxidised to K^+, the number of electron shells decreases by one, and the radius *R* decreases by approximately 2 Å. However, when there is no change in the number of shells, whether K^+ is further oxidised or K^0 is reduced, the changes in *R* are less pronounced. In reality, several potassium ions aside from the well-known K^+ exist as well-defined species. For instance, the simple anion K^- exists in solution,[42,43] in the solid state[42], and in the gas phase.[44,45] Monoatomic multiply charged cations K^{n+} ($n = 2, 3, 4$) have been recorded to exist in the gas phase,[46] while the K_2^{2-} dimer anion is known in the solid state.[47] More complex cluster cations K_n^+ ($5 < n < 200$) have been studied in the gas phase,[48] and clusters K_n^+ ($2 < n < 90$) in helium nanodroplets.[49] Cluster anions K_n^- ($n = 2 - 7$)[50] and K_n^- ($n = 2 - 19$)[45] are known from gas phase studies. These examples demonstrate how the average charge of a potassium atom can have very distinct values, covering the entire range, as reflected in Fig. 8. However, when potassium

clusters or nanoparticles are not species but substructures, it is to be expected that the average charge of a potassium atom is between 0 and 1. Computed data from *Ospadov et al*.[51] indicate an intrinsically sigmoidal charge-radius relationship for potassium. Consequently, the red sigmoidal curve in Figure 8 was constructed to graphically represent this trend, covering all experimentally known potassium charges. The curve was positioned at the most probable location in the scatterplot, and is described by Eq. (15).

$$R\,/\,\text{Å} = 3.7 - 3\frac{e^{2.6(Q-0.4)}}{e^{2.6(Q-0.4)}+1} \tag{15}$$

Most data points lay within the charge interval [0, 1], encompassing elementary potassium, potassium clusters, and numerous potassium compounds. The curve was further utilised to determine charges from radii for selected K–K dimers in biomacromolecules, using the ligand-based method 2 and the dimer-based method 2 (see Section 2.7). The blue linear regression line (Fig. 8) was constructed for this interval only, and is presented by Eq. (16) for 472 data points.

$$R\,/\,\text{Å} = 2.3437 - 0.71152Q \tag{16}$$

This equation was statistically significant at $\alpha = 0.05$ ($r = -0.5301$, $p < 0.001$). The line was later used to determine charges from radii for selected K–K dimers in biomacromolecules, via the ligand-based method 1 and the dimer-based method 1 (Section 2.7). The curve and the line in Fig. 8 intersect at $Q = 0.5$. The pronounced variance in the scatterplot arises from the the inclusion of data from various experimental and calculation procedures, aggregation states, and potassium forms (elementary, clusters, nanoparticles, potassium in inorganic, organic and biomacromolecular structures). Despite these variations and potential experimental and calculation errors, the sigmoidal trend remained evident. In various compounds, potassium does not always have a charge equal or close to 1, but is frequently fractional, as can be easily predicted from Fig. 8. Furthermore, variations in Q mean changes in the valence electron content, which in turn also affect its radius R.

3.4 Measuring radii and estimating charges for potassium in biomacromolecules

Four examples of biomacromolecular structures from the PDB database were selected: The crystal structure of Na^+,K^+-ATPase from *Squalus acanthias* (PDB: 5AVQ),[52] a protein molecule containing K ions, a K–K dimer (Fig. 9 left), and an isolated K ion; The crystal structure of a B-DNA dodecamer containing 5-hydroxymethyl cytosine (PDB: 4GLH),[53] a synthetic construct with one K–K dimer *per* macromolecule (Fig. 9 right); The crystal structure of a group II intron RNA molecule from *Oceanobacillus iheyensis* (PDB: 4FB0)[54] has 15 potassium ions and only one K–K dimer (Fig. 10 left); The most complex crystal structure was that of protein endonuclease Cas9 VRER from *Streptococcus pyogenes* in molecular complex with nucleic acids sgRNA and target DNA (PDB: 5B2T).[55] This complex possesses 8 potassium ions and one K–K dimer *per* complex unit (Fig. 10 right). Fig. 9 shows the complete binding coordination sphere of two K–K dimers, while the coordination spheres of the other two K–K dimers, presented in Fig. 10, are incomplete due to missing water molecules in the PDB files. Non-bonding interactions between K ions and the macromolecule were omitted for clarity. All four examples of K–K dimers showed that oxygen-based ligands are the most frequent. Some are bidentate or even bridging ligands. Water (W) appears to be a frequent ligand.

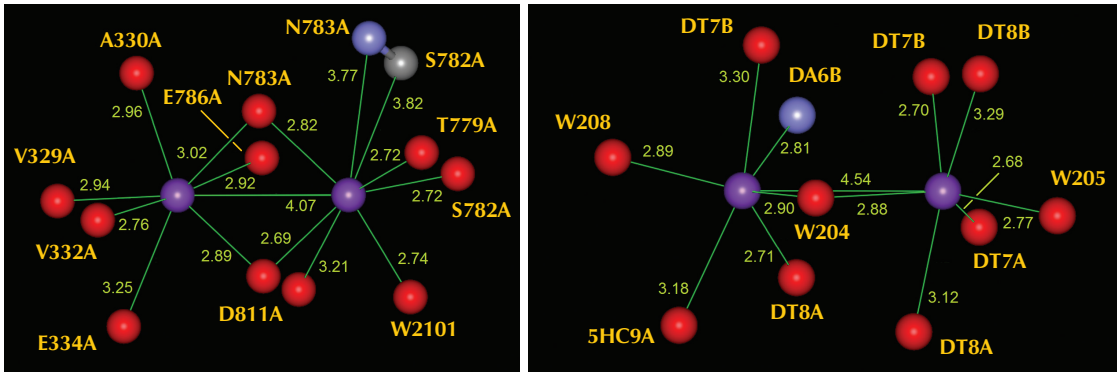

Fig. 9 – Potassium dimers within complete bonding coordination spheres in biomacromolecular structures. Left: K–K dimer (purple) surrounded by ligand atoms (O – red, N – blue, C – grey) in the crystal structure of a Na^+,K^+-ATPase (PDB: 5AVQ).[52] Right: K–K dimer (purple) surrounded by ligand atoms (O – red, N –- blue) in the crystal structure of a B-DNA dodecamer (PDB: 4GLH).[53] Bond lengths, ligand abbreviations, and numbering with chain names (A or B) are provided for each ligand atom bound to a K atom.

Slika 9 – Dimeri kalija unutar potpunih vezujućih koordinacijskih sfera u strukturama biomakromolekula. Lijevo: dimer K–K (ljubičasto) okružen atomima liganda (O – crveno, N – plavo, C – sivo) u kristalnoj strukturi Na^+,K^+-ATPaze (PDB: 5AVQ).[52] Desno: dimer K–K (ljubičasto) okružen atomima liganda (O – crveno, N – plavo) u kristalnoj strukturi dodekamera B-DNA (PDB: 4GLH).[53] Duljine veza, kratice i numeracije liganada s imenima lanaca (A ili B) dani su za svaki atom liganda vezan za atom K.

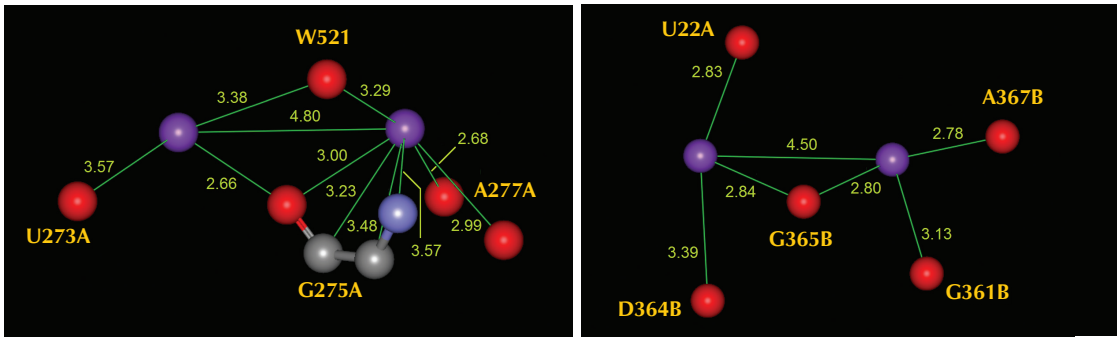

Fig. 10 – Potassium dimers within incomplete bonding coordination spheres in biomacromolecular structures. Left: K–K dimer (purple) surrounded by ligand atoms (O – red, N – blue, C – grey) in the crystal structure of a group II intron (PDB: 4FB0).[54] Right: K–K dimer (purple) surrounded by ligand atoms (O – red) in the crystal structure of a complex of endonuclease Cas9 with sgRNA and target DNA (PDB: 5B2T).[55] Bond lengths, ligand abbreviations, and numbering with chain names (A or B) are provided for each ligand atom bound to a K atom.

Slika 10 – Dimeri kalija unutar nepotpunih vezujućih koordinacijskih sfera u strukturama biomakromolekula. Lijevo: dimer K–K (ljubičasto) okružen atomima liganda (O – crveno, N – plavo, C – sivo) u kristalnoj strukturi introna grupe II (PDB: 4FB0).[54] Desno: dimer K–K (ljubičasto) okružen atomima liganda (O – crveno) u kristalnoj strukturi endonukleaze Cas9 s sgRNA i ciljnom DNA (PDB: 5B2T).[57] Duljine veza, kratice i numeracija liganada s imenima lanaca (A ili B) dani su za svaki atom liganda vezan za atom K.

Potassium ions in biomacromolecular structures (Figs. 9 and 10) originate from the use of solutions of ionic salts KCl,[52–56] KF,[52] and KSCN[55] during experimental procedures. When these salts are dissolved in water, the formation of hydrated K^+ ions with coordinate K–OH_2 bonds starts immediately,.[57] During hydration, 6–7 oxygen atoms are coordinated on a K atom.[58,59] It can be further presumed that, based on the oxygen electronegativity, the actual charge on K would be similar to that in ionic halides. However, when crystallisation occurs, the hydrated K ion undergoes dehydration and complexation with ligand groups of a macromolecule. Many of these ligand groups are not single-bonded oxygen atoms, as in water, but are oxygen, nitrogen, carbon, or other atoms involved in double or partial double bonds. These groups are relatively good electron donors, making the determination of potassium charge and radius in a biomacromolecule indeed meaningful.

The results of K–K dimer binding geometry measurements, and calculations of potassium charges and radii are presented in Table 5. The D_d values span a range of 0.7 Å. The radii values determined using different measurement methods show variations of up to 0.3 Å. For radii calculated using the ligand-based methods, due to incomplete bonding coordination spheres, additional water molecules were included (five for structure 4FB0 and four for structure 5B2T). Charge values cannot always be reliably calculated using the dimer method 1, because of underprediction even resulting in negative values. Variability in both charge and bond order values is evident but still reasonable, with no extreme value for any biomacromolecular structure. The best choice for all measured features is to use their average values. It can be concluded that the potassium atom has an average bonding radius in the range of 2.2–2.3 Å, and non-bonding radius between 2.4–2.6 Å. The average charge for potassium is small to medium, ranging from 0.3 to 0.5, indicating that ligand atoms donate a substantial amount of negative charge. This suggests that the K–K bond was formed with an average bond order of 0.5–0.7. Even if all K–K dimers in this study were analysed, the aforementioned conclusion would be similar in the qualitative sense.

Data for pure metal potassium were sourced from the literature:[23,60] the bond length in metallic state (4.54 Å, with half this value representing the metallic radius 2.27 Å), the covalent radius for single bond (1.96 Å), the Shannon effective ionic radius for coordination number 6 (1.38 Å), and the non-bonding or van der Walls radius (2.73 Å). The charge of a potassium atom in its pure metallic state can be approximated as 0.1, since it is known that sodium, a very similar metal, has this value for non-shared valence electrons.[61] The theoretical bond order of the metallic bond in potassium is 0.25. When comparing the average values of the features for the four dimers (Table 5) with corresponding values for metallic potassium, a certain geometrical similarity was observed between dimer bonds and the metallic bond in terms of bonding radii, and even non-bonding radii. However, the electronic features, including charges and bond orders, exhibited significant differences between the two types of bonds. Bond orders for K–K dimers were higher than those in the pure metal, but at the same time, the atoms in the metal had more valence electrons than the atoms in the dimers. This suggested that the bond in the dimers was not metallic, but somewhat similar to it. The dimer bonds were clearly not ionic, as the charges on K atoms were not close to 1, and the ionic radii for K for any coordination number were too small. Additionally, the frequent ligand atoms bound to K–K dimers (O, N, C atoms) could not be considered as ions. Furthermore, the dimer bonds were not typical covalent bonds. K atoms only receive fractional negative charge from their ligands. The covalent radius for K, as reported in the literature, is smaller than the obtained bonding radii.

Table 5 – Measured and calculated features of K–K dimers in four structures of biomacromolecules selected from the PDB database, compared to the state of the pure metal potassium

Tablica 5 – Mjerena i izračunata svojstva dimera K–K u četirima odabranim strukturama biomakromolekula iz baze podataka PDB, u usporedbi sa stanjem čistog metala kalija

Feature	Method	PDB: 5AVQ	PDB: 4GLH	PDB: 4FB0	PDB: 5B2T	Pure metal
D_d/Å	experimental	4.07	4.54	4.80	4.50	4.54
R/Å	ligand-based method 1	2.21	2.27	2.11	2.20	
	ligand-based method 2	2.21	2.27	2.11	2.20	
	dimer-based method 1	2.04	2.27	2.40	2.25	
	dimer-based method 2	2.04	2.27	2.40	2.25	
	dimer-based method 3	2.04	2.27	2.40	2.25	
	average	2.13	2.27	2.26	2.23	2.27
Q	ligand-based method 1	0.19	0.10	0.33	0.20	
	ligand-based method 2	0.39	0.36	0.44	0.40	
	dimer-based method 1	0.43	0.10	–	0.13	
	dimer-based method 2	0.48	0.36	0.30	0.37	
	dimer-based method 3	0.18	0.61	0.76	0.59	
	average	0.33	0.31	0.46	0.34	0.10
B	ligand-based method 1	0.81	0.90	0.67	0.80	
	ligand-based method 2	0.61	0.64	0.56	0.60	
	dimer-based method 1	0.57	0.90	–	0.87	
	dimer-based method 2	0.52	0.64	0.70	0.63	
	dimer-based method 3	0.72	0.39	0.24	0.41	
	average	0.65	0.69	0.54	0.66	0.25
R_{nb}/Å	contact-based method	2.54	2.42	2.50	2.59	2.73

Fig. 11 illustrates the geometric features of bonding and non-bonding radii for the dimer in the B-DNA dodecamer structure (PDB: 4GLH),[53] compared to the metallic, covalent, and ionic radius for potassium. In this case, the metallic radius was equal to the bonding radius, but this was merely coincidental and does not apply to other dimers in Table 5. The covalent radius from the literature is a fixed value, assuming that it can be normally used as it does not change significantly from one structure to another. In the case of potassium and other metals examined in this work, bonding radii varied, making fixed covalent radii less useful. As shown in Figure 11, the covalent radius was too small, while the ionic radius for K was even smaller, resulting in a large gap between the two hypothetical K^+ ions. This gap was consistent across all the dimers, as the K–K bond lengths were longer than twice the ionic radius for K. Furthermore, ligands, even when carrying formal non-zero charge (*e.g.*, containing carboxylate oxygen), are not strictly ionic compounds but covalent, frequently involved in certain π-electron delocalisation systems, such as peptide bonds –CO–NH–, amino-acid residues with partial double bonds, nucleobases, and phosphate groups in nucleic acids, among others. The selected K–K dimers analysed in this section indicated that none of the radii — metallic, covalent, or ionic — adequately described the K–K bonds. The bonding and non-bonding radii in Fig. 11 provide a more practical description of the K atoms' size in dimers. It is important to note, however, that these radii are hypothetical constructions, as K atoms have fractional

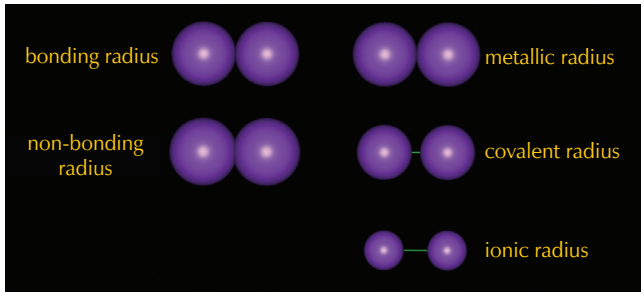

Fig. 11 – Potassium dimer from the crystal structure of a B-DNA dodecamer (PDB: 4GLH),[53] presented by bonding and non-bonding radii for K obtained in this work (left), and also by metallic, covalent, and ionic radii from literature (right)[23,60]

Slika 11 – Dimer kalija iz kristalne strukture dodekamera B-DNA (PDB: 4GLH),[53] prikazan veznim i neveznim radijusima za K koji su dobiveni u ovom radu (lijevo) te također metalnim, kovalentnim i ionskim radijusima iz literature (desno)[23,60]

charges only when bound to electron-donor atoms, and not as isolated atoms (where charges are integer values). In other words, the donor atoms donate electrons to two K^+ ions, which are brought into close proximity either by chance or through the action of ligands, especially bridging ligands. This enables the K ions to form a metavalent bond, borderline metavalent/covalent, or even a metavalent/metallic bond. Larger interatomic distances than those provided in Table 5 could represent weak or very weak bonds, or at least metallophilic interactions. The precise mechanism by which potassium, a non-transition metal, forms dimers in biomacromolecular structures in terms of atomic orbitals is beyond the scope of this study. However, it is known from the literature that 4s, 4p, and 3d orbitals of potassium, whether pure or hybridised, can participate in bonding within potassium compounds.[62–64]

3.5 Estimated charges for potassium in biomacromolecules in the metavalent bonding space

According to Table 5, the parameter $S = 0$, while T values are 1.30, 1.38, 1.08, and 1.28 for the K–K dimer in the PDB structures 5AVQ, 4GLH, 4FB0, and 5B2T, respectively. The more complex model of the K–K dimers, where the K atoms are analysed individually, is presented in Table 6. Differences in the R and Q values are evident for each dimer. As previously mentioned, the most reliable approach to estimating radii and charges involves utilising all five available methods. However, this was not possible in this case, resulting in $T > 0.05$, and S values consistently higher than those observed in the simple model.

The relationship between transferred electrons (T) and shared electrons (S) is presented by 181 data points in Fig. 12. It is based on a newly formed database compiled from various sources,[61,65–71] including textual, tabular, and pictorial records. The S and T data primarily represent binary and ternary inorganic compounds, along with chemical elements and organic compounds. For metallic potassium, the data were estimated using the data for alkali and alkaline earth metals. The data for the four selected K–K dimers in biomacromolecules were also added: the dimers analysed using the simple model lay along the vertical axis, while those from the more detailed model were more dispersed in the neighbouring region. The area of metavalent

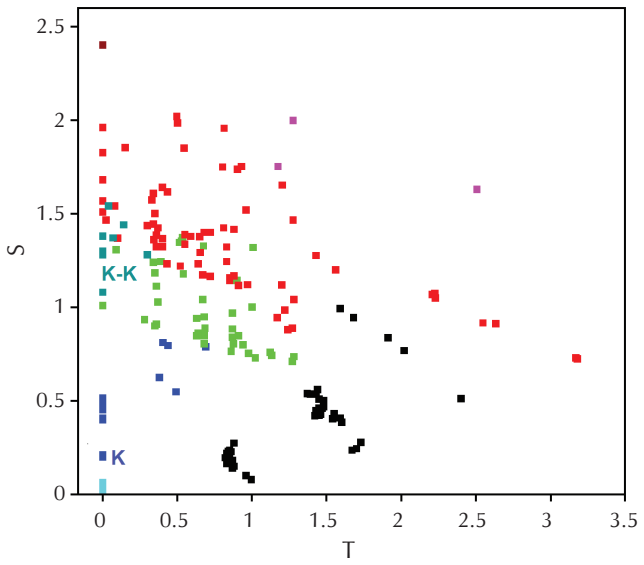

Fig. 12 – Transferred electrons (T) – shared electrons (S) scatterplot as the space of chemical bond types, based on 181 coloured data points. Legend: blue – metallic bonds; red – single covalent bonds; black – ionic bonds; green – metavalent bonds; magenta – hypervalent covalent bonds; brown – resonant covalent bonds; cyan – van der Waals bonds; teal – K–K bonds in biomacromolecules. The positions of metallic K and K–K dimers in biomacromolecules are specially marked in the scatterplot.

Slika 12 – Dijagram raspršenja preneseni elektroni (T) – dijeljeni elektroni (S) kao prostor za tipove kemijske veze, baziran na 181 podatkovnoj točki u boji. Legenda: plavo – metalne veze; crveno – jednostruke kovalentne veze; crno – ionske veze; zeleno – metavalentne veze; magenta – hipervalentne kovalentne veze; smeđe – rezonantne kovalentne veze; cijan – van der Waalsove veze; plavozeleno – veze K–K u biomakromolekulama. Položaji metalnog K i dimera K–K u biomakromolekulama posebno su označeni u dijagramu raspršenja.

bonds (green) lay between the regions of metallic bonds (blue, representing metallic elements and intermetallic compounds) and single covalent bonds (red), where some overlap occurred. The right end of the metavalent bond

Table 6 – Measured and calculated features of K atoms of the K–K dimers in four structures of biomacromolecules selected from the PDB database, compared to the state of pure metal potassium

Tablica 6 – Mjerena i izračunata svojstva atoma K u dimerima K–K u četirima odabranim strukturama biomakromolekula iz baze podataka PDB, u usporedbi sa stanjem čistog metala kalija

Feature	Method	PDB: 5AVQ	PDB: 4GLH	PDB: 4FB0	PDB: 5B2T	Pure metal
R/Å	ligand-based method 1	2.30, 2.12	2.25, 2.30	2.30, 1.98	2.15, 2.27	
	ligand-based method 2	2.30, 2.12	2.25, 2.30	2.30, 1.98	2.15, 2.27	
Q	ligand-based method 1	0.06, 0.31	0.13, 0.06	0.06, 0.51	0.27, 0.20	
	ligand-based method 2	0.35, 0.39	0.37, 0.35	0.35, 0.51	0.43, 0.36	
	average	0.21, 0.35	0.25, 0.21	0.21, 0.51	0.35, 0.28	0.10
T	charge-based estimation	0.14	0.04	0.30	0.07	0
S	charge-based estimation	1.44	1.54	1.28	1.37	0.21

area touches the area associated with inorganic bonds (black).

The position of the K–K bonds can be named as the left side of the metavalent area, as *S* is small or equal to zero. Thus, the K–K bonds could be classified as metavalent bonds or borderline metavalent/single covalent bonds. It is highly probable that all 31 metals from the all metals database, when analysed for partial atomic charges, would be positioned as metavalent bonds or borderline metavalent/covalent or even metavalent/metallic bonds, because the area of the metavalent bonding is rather narrow. It is unlikely that such metal-metal bonds would occupy the space of a typical single covalent or the metallic bond. The difference between the K–K bond in metallic K and the K–K bonds in the dimers within biomacromolecules is considerable, with the minimum being 0.87 and the maximum 1.33 units of *S*.

What role do K–K or other M–M dimers play in biomacromolecules? The bonds in such dimers are typically weaker compared to single covalent bonds, which is why they can be classified as metavalent, borderline metavalent/covalent, or metavalent/metallic bonds. Visual inspection of macromolecular crystal structures containing the four selected and other K–K dimers and several other M–M dimers, revealed that these dimers were always positioned in semi-flexible macromolecular regions, between two or more rigid or semi-flexible parts of a biomacromolecule, or even linking two biomacromolecules. This suggests that all dimers contribute to the stability and flexibility of the biomacromolecular structures, and several of these dimers participate in chemical reactions, such as the Fe_2S_2 dimer in electron transfer reactions.[16]

4 Conclusion

This study presents four structural pieces of evidence for the existence of metavalent, borderline metavalent/covalent, or metavalent/metallic bonds in homodinuclear metal clusters within biomacromolecular structures. The findings can be summarized as follows.

1) In total, 31 metals from various parts of the periodic table were found to form 565 dimers in the crystal structures of biomacromolecules: *s*-block metals (Li, Na, Mg, K, Ca, Rb. Sr, Cs and Ba), transition metals (V, Mn, Fe, Co, Ni, Cu, Zn, Mo, Ru, Rh, Pd, Ag, Cd, Au and Hg), *p*-block metals (Ga, Tl and Pb), and lanthanides (La, Eu, Dy and Ho). These findings indicate that any metal can form dimers in biomacromolecular structures.
2) Statistical analysis of empirical and theoretical distributions for three quantities — bond length relative to twice the van der Waals radius, bond length and bond order relative to pure metal — showed significant diversity in metal-metal bonds in dimers within biomacromolecules. Additionally, the distributions were non-normal, with metals dispersed in all parts of the theoretical curves. In other words, all metals behave similarly, and metal-metal bonds cannot be classified as metallic, covalent, or ionic. The best classification for these bonds is metavalent, borderline metavalent/covalent, or metavalent/metallic, all caused by the action of various donor ligands bound to metallic ions.
3) The bonds *per* atom-bond length deviation relationship for 761 silver clusters in biomacromolecules, organics and organometallics, inorganics and intermetallics, and other silver structures revealed that bond length deviation decreased curvilinearly with the increase in bonds *per* atom, while Ag–Ag bonds acquired an increasingly metallic character. This phenomenon was more pronounced in biomacromolecules, less so in organics and organometallics, and least evident in inorganics and intermetallics. Metavalent bonds, or borderline metavalent/covalent, or metavalent/metallic bonds, appeared to exist for values of bonds *per* atom ranging from around 0.5 for dimers to 3, when half of the binding coordination sphere was occupied by Ag atoms. It is supposed that dimers of other metals in biomacromolecules exhibit similar behaviour to silver dimers.
4) The partial atomic charge-radius relationship for 515 potassium clusters indicated that potassium atoms, when bound to biomacromolecules, acquire a certain amount of negative charge, allowing them to form metavalent bonds or, at least borderline metavalent/covalent, or metavalent/metallic bonds. As the charge changed, the bonding and non-bonding radii of potassium atoms also changed. Charges and radii for the four selected potassium dimers in crystal structures of biomacromolecules were determined from structural data. The results strongly indicated that the bonds of potassium dimers within biomacromolecules were not typically covalent, ionic, or metallic, but rather metavalent, borderline metavalent/covalent, or metavalent/metallic bonds. It is expected that dimers of other metals in biomacromolecules exhibit similar behaviour.
5) Both simple and complex charge analysis of the selected potassium dimers, in terms of the transferred electrons – shared electrons relationship, showed that the dimer bonds were located in the left part of the metavalent bonding area. It is expected that the bonds in dimers of all the studied metals in biomacromolecules will fall into this area or be borderline metavalent/covalent or even metavalent/metallic bonds.

Homonuclear dimers with multiple metal-metal bonds, which are of covalent nature (resonant, hypervalent, typical multiple, *etc.*), differ significantly from metallic bonds and are not considered metavalent. Such bonds were not included in this study.

List of abbreviations and symbols
Popis kratica i simbola

α – statistical significance level
– razina statističke značajnosti

B – bond order for K–K distance, defined as 1 – *Q*, for *Q* values between 0 and 1
– red veze za udaljenost K–K, definirana kao 1 – *Q*, za vrijednosti *Q* između 0 i 1

β – average number of Ag–Ag bonds *per* Ag atom
– prosječan broj veza Ag–Ag po atomu Ag

β_{max} – maximum value of the number β
– najveća vrijednost broja β

β_{min} – minimum value of the number β
– najmanja vrijednost broja β

COD ID – identification number from the Crystallography Open Database
– identifikacijski broj iz baze podataka Crystallography Open Database

D – thickness of silver thin film in Å units
– debljina tankog filma srebra u jedinicama Å

Δ – bond length deviation of an Ag–Ag bond from the standard Ag–Ag bond length for bulk silver at room temperature and normal pressure (2.889 Å)
– odstupanje duljine veze Ag–Ag od duljine standardne veze Ag–Ag za metalno srebro na sobnoj temperaturi i kod normalnog tlaka (2.889 Å)

d – bond length in Å units
– duljina veze u jedinicama Å

δ – relative bond length of a M–M dimer, defined as fraction $d/2r_{vdW}$
– relativna duljina veze dimera M–M, definirana kao omjer $d/2r_{vdW}$

d(Ag...Ag) – interatomic Ag–Ag distance for normal, weak, or very weak bond, argentophillic interaction, or contact, in Å units
– međuatomske udaljenosti Ag–Ag za normalnu, slabu ili vrlo slabu vezu, argentofilnu interakciju ili kontakt, u jedinicama Å

d_{av} – average interatomic Ag–Ag distance, in Å units
– prosječna međuatomska udaljenost Ag–Ag, u jedinicama Å

D_d – K–K bond length in Å unit
– duljina veze K–K u jedinicama Å

d_{max} – maximum bond length, given as a range for weak M–M bonds, in Å units
– najveća duljina veze, dana kao raspon za slabe veze M–M, u jedinicama Å

Δ_{max} – maximum of deviation Δ, in Å units
– najveća vrijednost odstupanja Δ, u jedinicama Å

Δ_{min} – minimum of deviation Δ, in Å units
– najmanja vrijednost odstupanja Δ, u jedinicama Å

DNA – deoxyribonucleic acid
– deoksiribonukleinska kiselina

d_0 – bond length in pure crystalline metal, in Å units
– duljina veze u čistom kristalnom metalu, u jedinicama Å

d_i – interatomic distance of the *i*-th Ag–Ag bond, interaction or contact, in Å units
– međuatomska udaljenost *i*-te veze, interakcije ili kontakta Ag–Ag, u jedinicama Å

δ_0 – relative M–M bond length in pure crystalline metal, defined as fraction $d_0/2r_{vdW}$
– relativna duljina veze M–M u čistom kristalnom metalu, definirana kao omjer $d_0/2r_{vdW}$

E – atom of any chemical element except K
– atom bilo kojeg kemijskog elementa osim K

E–E – chemical bond between two atoms of the element E
– kemijska veza između dvaju atoma elementa E

E–K – chemical bond between atoms of the elements E and K
– kemijska veza između atoma elemenata E i K

ε – difference in relative M–M bond lengths, defined as $\delta - \delta_0$
– razlika relativnih duljina veza M–M, definirana kao $\delta - \delta_0$

F – absolute frequency
– apsolutna frekvencija

h – height of a cylindrical silver nanoparticle, in Å units
– visina cilindričke nanočestice srebra, u jedinicama Å

j – non-integer coefficient in expression for calculation of deviation Δ from β value
– necijeli koeficijent u izrazu za računanje odstupanja Δ iz vrijednosti β

k – non-integer coefficient in expression for calculation of deviation Δ from β value
– necijeli koeficijent u izrazu za računanje odstupanja Δ iz vrijednosti β

l – non-integer coefficient in expression for calculation of deviation Δ from β value
– necijeli koeficijent u izrazu za računanje odstupanja Δ iz vrijednosti β

λ – bond order of dimer M–M
– red veze dimera M–M

λ_0 – bond order of a pure crystalline metal
– red veze čistog kristalnog metala

λ_c – calculated bond order of a pure crystalline metal, using polynomial regression
– proračunati red veze čistog kristalnog metala, upotrebom polinomske regresije

m – non-integer coefficient in expression for calculation of deviation Δ from β value
– necijeli koeficijent u izrazu za računanje odstupanja Δ iz vrijednosti β

M – common designation for metal or metal atom
– uobičajena oznaka za metal ili atom metala

M–M – homonuclear metal-metal bond or metal-metal dimer
– homonuklearna veza metal-metal ili dimer metal-metal

M_2 – homonuclear metal-metal dimer
– homonuklearni dimer metal-metal

μ – difference in bond orders, defined as $\lambda - \lambda_c$
– razlika redova veza, definirana kao $\lambda - \lambda_c$

n – total number of all Ag–Ag bonds, interactions, and contacts, or the number of atoms in K clusters
– ukupan broj svih veza, interakcija i kontakata Ag–Ag ili broj atoma u klasterima K

N – number of entries (Ag clusters) with normal Ag–Ag bonds, in a module of the silver database
– broj zapisa (klastera srebra) s normalnim vezama Ag–Ag, u modulu baze podataka za srebro

ν – degree of polynomials for bond length – bond order relationships for M–M dimers
– stupanj polinoma za odnose između duljine veze i reda veze za dimere M–M

n_b – true number of Ag–Ag bonds
– pravi broj veza Ag–Ag

N_{tot} – total number of entries (Ag clusters) in a module of the silver database
– ukupan broj zapisa (klastera srebra) u modulu baze podataka za srebro

N_w – number of entries (Ag clusters) with weak and very weak Ag–Ag bonds, interactions and contacts, in a module of the silver database
– broj zapisa (klastera srebra) sa slabim i vrlo slabim vezama, interakcijama te kontaktima Ag–Ag, u modulu baze podataka za srebro

p – probability in *F*-test for regression equation
– vjerojatnost u *F*-testu za regresijsku jednadžbu
PDB – Protein Data Bank, a structural database for proteins and other macromolecules
– strukturna banka podataka za proteine i druge makromolekule Protein Data Bank
Q – average partial atomic charge of K atoms in K–K dimer or larger K cluster
– prosječan parcijalni atomski naboj atoma K u dimeru K–K ili u većem klasteru kalija
r – Pearson correlation coefficient in *F*-test for regression equation
– Pearsonov koeficijent korelacije u *F*-testu za regresijsku jednadžbu
R – bonding radius of K atom in K–K dimer or larger K cluster, in Å atoms
– vezni radijus atoma K u dimeru K–K ili u većem klasteru kalija, u jedinicama Å
r_{cov1} – molecular single bond covalent radius, in Å atoms
– molekulski kovalentni radijus jednostruke veze, u jedinicama Å
r_{cov2} – molecular double bond covalent radius, in Å atoms
– molekulski kovalentni radijus dvostruke veze, u jedinicama Å
r_{cov3} – molecular triple bond covalent radius, in Å atoms
– molekulski kovalentni radijus trostruke veze, u jedinicama Å
RNA – ribonucleic acid
– ribonukleinska kiselina
R_{nb} – non-bonding radius of K atom in K–K dimer or larger K cluster, in Å units
– nevezni radijus atoma K u dimeru K–K ili u većem klasteru kalija, u jedinicama Å
r_{vdW} – van der Waals radius in Å units
– van der Waalsov radijus u jedinicama Å
ρ – radius of spherical or cylindrical silver nanoparticle, in Å units
– radijus sferičke ili cilindričke nanočestice srebra, u jedinicama Å
S – amount of shared electrons between two atoms in the chemical bond
– količina elektrona koju dijele dva atoma u kemijskoj vezi
T – amount of electrons transferred from one atom to another in the chemical bond
– količina elektrona koja je prenesena s jednog atoma na drugi u kemijskoj vezi
u – weighting factor for silver nanostructures
– težinski faktor za nanostrukture srebra
w – weighting factor for a particular Ag–Ag bond or interaction
– težinski faktor za pojedinu vezu ili interakciju Ag–Ag
w_i – weighting factor for the *i*-th Ag–Ag bond or interaction
– težinski faktor za *i*-tu vezu ili interakciju Ag–Ag
X – common designation for some elements bound to K, e.g., O, N, C
– zajednička oznaka za neke elemente vezane za K, na primjer O, N, C
Z – atomic number
– atomski broj

References
Literatura

1. *M. Kaupp, H. G. von Schnering*, Origin of the Unique Stability of Condensed-Phase Hg_2^{2+}. An ab Initio Investigation of M^I and M^{II} Species (M = Zn, Cd, Hg), Inorg. Chem. **33** (1994) 4179–4185, doi: https://doi.org/10.1021/ic00096a049.
2. *M. S. Wickleder*, $AuSO_4$: A True Gold(II) Sulfate with an Au_2^{4+} Ion, Z. Anorg. Allg. Chem. **627** (2001) 2112–2114, doi: https://doi.org/10.1002/1521-3749(200109)627:9<2112::AID-ZAAC2112>3.0.CO;2-2.
3. *P. Kusch, M. M. Hessel,* An analysis of the $B^1\Pi_u$–$X^1\Sigma^+_g$ band system of Na_2, J. Chem. Phys. **68** (1978) 2591–2606, doi: https://doi.org/10.1063/1.436117.
4. *F. A. Cotton, E. A. Hillard, C. A. Murillo*, The First Dirhodium Tetracarboxylate Molecule without Axial Ligation: New Insight into the Electronic Structures of Molecules with Importance in Catalysis and Other Reactions, J. Am. Chem. Soc. **124** (2002) 5658–5660, doi: https://doi.org/10.1021/ja025760j.
5. *R. H. Huang, D. L. Ward, J. L. Dye,* Alkali-Metal-Anion Dimers and Chains in Alkalide Structures, J. Am. Chem. Soc. **111** (1989) 5707–5708, doi: https://doi.org/10.1021/ja00197a031.
6. *T. Knöfel, N. Sträter,* X-ray structure of the *Escherichia coli* periplasmic 5′-nucleotidase containing a dimetal catalytic site, Nat. Struct. Biol. **6** (1999) 448–453, doi: https://doi.org/10.1038/8253.
7. *J. Duan, M. Senger, J. Esselborn, V. Engelbrecht, F. Wittkamp, U.-P. Apfel, E. Hofmann, S. T. Stripp, T. Happe, M. Winkler,* Crystallographic and spectroscopic assignment of the proton transfer pathway in [FeFe]-hydrogenases, Nat. Commun. **9** (2018) 4726, doi: https://doi.org/10.1038/s41467-018-07140-x.
8. *V. L. Pecorato, Z. Guo* (eds.), Comprehensive Inorganic Chemistry III, Volume 2, Elsevier, Amsterdam, 2023.
9. *W. Kaim, B. Schwederski, A. Klein,* Bioinorganic Chemistry: Inorganic Elements in the Chemistry of Life – An Introduction and Guide, 2nd ed., Wiley, Chichester, 2013.
10. *T. L. Yusuf, S. A. Ogundare, M. N. Pillay, W. E. van Zyl,* Heptanuclear Silver Hydride Clusters as Catalytic Precursors for the Reduction of 4-Nitrophenol, Molecules **27** (2022) 5223, doi: https://doi.org/10.3390/molecules27165223.
11. *I. G. Powers, C. Uyeda,* Metal−Metal Bonds in Catalysis, ACS Catal. **7** (2017) 936–958, doi: https://doi.org/10.1021/acscatal.6b02692.
12. *Y. Wang, Y. Kuang, Y. Wang*, $Rh_2(esp)_2$-catalyzed allylic and benzylic oxidations, Chem. Commun. **51** (2015) 5852, doi: https://doi.org/10.1039/c4cc10336j.
13. *V. Porto, D. Buceta, B. Domínguez, C. Carneiro, E. Borrajo, M. Fraile, N. Davila-Ferreira, I. R. Arias, J. M. Blanco, M. C. Blanco, J. M. Devida, L. J. Giovanetti, F. G. Requejo, J. C. Hernández-Garrido, J. J. Calvino, M. López-Haro, G. Barone, A. M. James, T. García-Caballero, D. M. González-Castaño, M. Treder, W. Huber, A. Vidal, M. P. Murphy, M. López-Quintela, F. Domínguez,* Silver Clusters of Five Atoms as Highly Selective Antitumoral Agents Through Irreversible Oxidation of Thiols, Adv. Funct. Mater. **32** (2022) 2113028, doi: https://doi.org/10.1002/adfm.202113028.

14. *Q. Wang, S.-L. Dong, D.-D. Tao, Z. Li, Y.-B. Jiang*, Ag(I)-thiolate coordination polymers: Synthesis, structures and applications as emerging sensory ensembles, Coord. Chem. Rev. **432** (2021) 213717, doi: https://doi.org/10.1016/j.ccr.2020.213717.
15. *A. Gonzàlez-Rosell, C. Cerretani, P. Mastracco, T. Vosch, S. M. Copp*, Structure and luminescence of DNA-templated silver clusters, Nanoscale Adv. **3** (2021) 1230, doi: https://doi.org/10.1039/d0na01005g.
16. *A. D. Read, R. E. T. Bentley, S. L. Archer, K. J. Dunham-Snary,* Mitochondrial iron–sulfur clusters: Structure, function, and an emerging role in vascular biology, Redox Biol. **47** (2021) 102164, doi: https://doi.org/10.1016/j.redox.2021.102164.
17. *M. Wuttig, V. L. Deringer, X. Gonze, C. Bichara, J.-Y. Raty*, Incipient Metals: Functional Materials with a Unique Bonding Mechanism, Adv. Mater. **30** (2018) 1803777, doi: https://doi.org/10.1002/adma.201803777.
18. *L. Guarneri, S. Jakobs, A. von Hoegen, S. Maier, M. Xu, M. Zhu, S. Wahl, C. Teichrib, Y. Zhou, O. Cojocaru-Mirédin, M. Raghuwanshi, C.-F. Schön, M. Drögeler, C. Stampfer, R. P. S. M. Lobo, A. Piarristeguy, A. Pradel, J.-Y. Raty, M. Wuttig,* Metavalent Bonding in Crystalline Solids: How Does It Collapse?, Adv. Mater. **33** (2021) 2102356, doi: https://doi.org/10.1002/adma.202102356.
19. *S. Shaik, D. Danovich, J. M. Galbraith, B. Braïda, W. Wu, P. C. Hiberty,* Angew. Chem. Int. Ed. **59** (2020) 984–1001, doi: https://doi.org/10.1002/anie.201910085.
20. URL: https://www.rcsb.org/ (July 7, 2024)
21. *ViewerLite 4.2*, Accelrys, Inc., San Diego, CA, 2001.
22. *Mercury 3.6*, Cambridge Crystallographic Data Centre, Cambridge, 2015.
23. URL: https://www.webelements.com/ (July 7, 2024).
24. URL: http://www.crystallography.net/cod/ (July 21, 2024).
25. URL: https://arachnoid.com/polysolve/ (July 21, 2024).
26. *JASP 0.18.3*. University of Amsterdam, Amsterdam, 2024.
27. *Pirouette 4.5 rev 1*, Infometrix, Inc., Bothell, WA, 2014.
28. *M. E. Straumanis*, Neubestimmung der Gitterparameter, Dichten und thermischen Ausdehnungskoeffizienten von Silber und Gold, und Vollkommenheit der Struktur, Monatsh. Chem. **102** (1971) 1377–1386, doi: https://doi.org/10.1007/BF00917194.
29. *I.-K. Suh, H. Ohta, Y. Waseda*, High-temperature thermal expansion of six metallic elements measured by dilatation method and X-ray diffraction, J. Mater. Sci. **23** (1988) 757–760, doi: https://doi.org/10.1007/BF01174717.
30. *S. Sen, S. K. Halder, S. P. S. Gupta,* An x-ray line shift analysis in vacuum-evaporated silver films, J. Phys. D **6** (1973) 1978–1985, doi: https://doi.org/10.1088/0022-3727/6/17/304.
31. URL: https://www.ccdc.cam.ac.uk/structures/ (July 21, 2024).
32. URL: https://rruff.geo.arizona.edu/AMS/amcsd.php (July 21, 2024).
33. *Scilab 5.5.2*, Scilab Enterprises S. A. S., Orsay, 2015.
34. URL: https://mycurvefit.com/ (July 2, 2024).
35. URL: http://vassarstats.net/corr_big.html (June 22, 2024).
36. *O. C. Gagné, F. C. Hawthorne*, Bond-length distributions for ions bonded to oxygen: alkali and alkaline-earth metals, Acta Cryst. B **72** (2016) 602–625, doi: https://doi.org/10.1107/S2052520616008507.
37. *Yu. V. Nelyubina, K. A. Lyssenko, M. Yu. Antipin,* Estimation of the Energy of Coordination K–O Bonds in a Potassium Hydrophthalate Crystal on the Basis of Electron-Density Distribution Analysis, Crystallogr. Rep. **53** (2008) 192–198, doi: https://doi.org/10.1134/S1063774508020053.
38. *I. Kobrsi, W. Zheng, J. E. Knox, M. J. Heeg, H. B. Schlegel, C. H. Winter,* Experimental and Theoretical Study of the Coordination of 1,2,4-Triazolato, Tetrazolato, and Pentazolato Ligands to the $[K(18\text{-crown-}6)]^+$ Fragment, Inorg. Chem. **45** (2006) 8700–8710, doi: https://doi.org/10.1021/ic061256u.
39. *G. Berionni, P. Mayer, H. Mayr,* Potassium [1-(tert-butoxycarbonyl)-1*H*-indol-3-yl]trifluoroborate hemihydrate, Acta Cryst. E **68** (2012) m551–m552, doi: https://doi.org/10.1107/S1600536812014225.
40. *C. Cerretani, M. B. Liisberg, V. Rück, J. Kondo, T. Vosch*, The effect of inosine on the spectroscopic properties and crystal structure of a NIR-emitting DNA-stabilized silver nanocluster, Nanoscale Adv. **4** (2022) 3212, doi: https://doi.org/10.1039/d2na00325b.
41. *Y. Chen, X. Yan, H. Geng, X. Sheng, L. Zhang, H. Wang, J. Li, Y. Cao, X. Pan*, Prediction of Stable Ground-State Binary Sodium-Potassium Interalkalis under High Pressures, Inorg. Chem. **60** (2021) 124–129, doi: https://doi.org/10.1021/acs.inorgchem.0c02506.
42. *N. C. Pyper, P. P. Edwards,* Metallization of Alkali Anions in Condensed Phases, J. Am. Chem. Soc. **122** (2000) 5092–5099, doi: https://doi.org/10.1021/ja993644j.
43. *P. P. Edwards, A. S. Ellaboudy, D. M. Holton,* NMR spectrum of the potassium anion K^-, Nature **317** (1985) 242–244, doi: https://doi.org/10.1038/317242a0.
44. *K. T. Andersson, J. Sandström, I. Yu. Kiyan, D. Hanstorp, D. J. Pegg,* Measurement of the electron affinity of potassium, Phys. Rev. A **62** (2000) 022503, doi: https://doi.org/10.1103/PhysRevA.62.022503.
45. *J. G. Eaton, L. H. Kidder, H. W. Sarkas, K. M. McHugh, K. H. Bowen,* Photoelectron Spectroscopy of Alkali Metal Cluster Anions, in P. Jena, S. N. Khanna, B. K. Rao, B.K. (eds.), Physics and Chemistry of Finite Systems: From Clusters to Crystals, NATO ASI Series, vol 374, Springer, Dordrecht, 1992, pp. 493–507, doi: https://doi.org/10.1007/978-94-017-2645-0_65.
46. *M. A. Khalal, J. Soronen, K. Jänkälä, S.-M. Huttula, M. Huttula, J.-M. Bizau, D. Cubaynes, S. Guilbaud, K. Ito, L. Andric, J. Feng, P. Lablanquie, J. Palaudoux, F. Penent,* Multielectron spectroscopy: energy levels of K^{n+} and Rb^{n+} ions (n = 2, 3, 4), J. Phys. B **50** (2017) 225003, doi: https://doi.org/10.1088/1361-6455/aa90d6.
47. *R. H. Huang, D. L. Ward, J. L. Dye*, Alkali-Metal-Anion Dimers and Chains in Alkalide Structures, J. Am. Chem. Soc. **111** (1989) 5707–5708, doi: https://doi.org/10.1021/ja00197a031.
48. *C. Brechignac, Ph. Cahuzac, F. Carlier, M. de Frutos, J. Leygnier,* Cohesive energies of K_n^+ ($5 < n < 200$) from photoevaporation experiments, J. Chem. Phys. **93** (1990) 7449–7456, doi: https://doi.org/10.1063/1.459418.
49. *L. A. der Lan, P. Bart, C. Leidlmair, H. Schöbel, S. Denifl, T. D. Märk, A. M. Ellis, P. Scheier,* Submersion of potassium clusters in helium nanodroplets, Phys. Rev. B **85** (2012) 115414, doi: https://doi.org/10.1103/PhysRevB.85.115414.
50. *K. M. McHugh, J. G. Eaton, G. H. Lee, H. W. Sarkas, L. H. Kidder, J. T. Snodgrass, M. R. Manaa, K. H. Bowen,* Photoelectron spectra of the alkali metal cluster anions: Na_n^- (n = 2−5), K_n^- (n = 2−7), Rb_n^- (n = 2−3), and Cs_n^- (n = 2−3), J. Chem. Phys. **91** (1989) 3792, doi: https://doi.org/10.1063/1.456861.
51. *E. Ospadov, J. Tao, V. N. Staroverov, J. P. Perdew*, Visualizing atomic sizes and molecular shapes with the classical turning surface of the Kohn–Sham potential, Proc. Natl. Acad. Sci. USA **115** (2018) E11578–E11585, doi: https://doi.org/10.1073/pnas.1814300115.

52. *H. Ogawa, F. Cornelius, A. Hirata, C. Toyoshima,* Sequential substitution of K^+ bound to Na^+,K^+-ATPase visualized by X-ray crystallography, Nat. Commun. **6** (2015) 8004, doi: https://doi.org/10.1038/ncomms9004.
53. *D. Renciuk, O. Blacque, M. Vorlickova, B. Spingler,* Crystal structures of B-DNA dodecamer containing the epigenetic modifications 5-hydroxymethylcytosine or 5-methylcytosine, Nucleic Acids Res. **41** (2013) 9891–9900, doi: https://doi.org/10.1093/nar/gkt738.
54. *M. Marcia, A. M. Pyle,* Visualizing Group II Intron Catalysis through the Stages of Splicing, Cell **151** (2012) 497–507, doi: https://doi.org/10.1016/j.cell.2012.09.033.
55. *S. Hirano, H. Nishimasu, R. Ishitani, O. Nureki,* Structural Basis for the Altered PAM Specificities of Engineered CRISPR-Cas9, Mol. Cell **61** (2016) 886–894, doi: https://doi.org/10.1016/j.molcel.2016.02.018.
56. *N. Toor, K. S. Keating, S. D. Taylor, A. M. Pyle,* Crystal Structure of a Self-Spliced Group II Intron, Science **320** (2008) 77–82, doi: https://doi.org/10.1126/science.1153803.
57. *J. Lin, Y. Xiao, Q. Zhao, W. Qu, H. Huang, T. Zhou, Q. Wu, H. Mao*, Mechanism of surface hydration of potassium carbonate: Insights from first principles simulations, Appl. Surf. Sci. **512** (2020) 145726, doi: https://doi.org/10.1016/j.apsusc.2020.145726.
58. *Y. Liu, H. Lu, Y. Wu, T. Hu, Q. Li*, Hydration and coordination of K^+ solvation in water from *ab initio* molecular-dynamics simulation, J. Chem. Phys. **132** (2010) 124503, doi: https://doi.org/10.1063/1.3369624.
59. *T. W. Whitfield, S. Varma, E. Harder, G. Lamoureux, S. B. Rempe, B. Roux*, Theoretical Study of Aqueous Solvation of K^+ Comparing ab Initio, Polarizable, and Fixed-Charge Models, J. Chem. Theory Comput. **3** (2007) 2068–2082, doi: https://doi.org/10.1021/ct700172b.
60. *R. D. Shannon,* Revised Effective Ionic Radii and Systematic Studies of Interatomic Distances in Halides and Chalcogenides, Acta Cryst. A **32** (1976) 751–767, doi: https://doi.org/10.1107/S0567739476001551.
61. *J.-Y. Raty, M. Schumacher, P. Golub, V. L. Deringer, C. Gatti, M. Wutt*ig, A Quantum-Mechanical Map for Bonding and Properties in Solids, Adv. Mater. **31** (2019) 1806280, doi: https://doi.org/10.1002/adma.201806280.
62. *G. Chiappe, E. Louis, A. Guijarro, E. San-Fabián, J. A. Vergés*, The role of potassium orbitals in the metallic behavior of K_3picene, Phys. Rev. B **90** (2014) 035109, doi: https://doi.org/10.1103/PhysRevB.90.035109.
63. *N. Guo, H. Xue, R. Ren, J. Sun, T. Song, H. Dong, Z. Zhao, J. Zhang, Q. Wang, L. Wu*, S-Block Potassium Single-atom Electrocatalyst with K–N_4 Configuration Derived from K^+/Polydopamine for Efficient Oxygen Reduction, Angew. Chem. Int. Ed. **62** (2023) e202312409, doi: https://doi.org/10.1002/anie.202312409.
64. *F. Xu, Z. Huang, P. Hu, Y. Chen, L. Zheng, J. Gaoa, X. Tang*, The promotion effect of isolated potassium atoms with hybridized orbitals in catalytic oxidation, Chem. Commun. **51** (2015) 9888, doi: https://doi.org/10.1039/c5cc02476e.
65. *B. J. Kooi, M. Wuttig,* Chalcogenides by Design: Functionality through Metavalent Bonding and Confinement, Adv. Mater. **32** (2020) 1908302, doi: https://doi.org/10.1002/adma.201908302.
66. *W. Zhang, H. Zhang, S. Sun, X. Wang, Z. Lu, X. Wang, J.-J. Wang, C. Jia, C.-F. Schön, R. Mazzarello, E. Ma, M. Wuttig,* Metavalent Bonding in Layered Phase-Change Memory Materials, Adv. Sci. **10** (2023) 2300901, doi: https://doi.org/10.1002/advs.202300901.
67. *Y. Cheng, S. Wahl, M. Wuttig,* Metavalent Bonding in Solids: Characteristic Representatives, Their Properties, and Design Options, Phys. Status Solidi RRL **15** (2020) 2000482, doi: https://doi.org/10.1002/pssr.202000482.
68. *D. Kim, Y. Kim, J.-S. Oh, C. Lee, H. Lim, C.-W. Yang, E. Sim, M.-H. Cho*, Conversion between metavalent and covalent bond in metastable superlattices composed of 2D and 3D sublayers, ACS Nano **16** (2022) 20758–20769, doi: https://doi.org/10.1021/acsnano.2c07811.
69. *M. Wuttig, C.-F. Schön, D. Kim, P. Golub, C. Gatti, J.-Y. Raty, B. J. Kooi, A. M. Pendás, R. Arora, U. Waghmare*, Metavalent or Hypervalent Bonding: Is There a Chance for Reconciliation?, Adv. Sci. **11** (2024) 2308578, doi: https://doi.org/10.1002/advs.202308578.
70. *P. C. Müller, S. R. Elliott, R. Dronskowski, R. O. Jones*, Chemical bonding in phase-change chalcogenides, J. Phys. Condens. Matter **36** (2024) 325706, doi: https://doi.org/10.1088/1361-648X/ad46d6.
71. *X. Zhang, Y. Guo, D. Chu, J. Robertson*, Enhanced photovoltaic properties of halide perovskites due to multi-centered X–B–X bonding and p–p orbital coupling, J. Appl. Phys. **133** (2023) 115701, doi: https://doi.org/10.1063/5.0139458.
72. *J.-Y. Ratya, C. Bichara, C.-F. Schön, C. Gatti, M. Wuttig*, Tailoring chemical bonds to design unconventional glasses, Proc. Natl. Acad. Sci. USA **121** (2024) e2316498121, doi: https://doi.org/10.1073/pnas.2316498121.

SAŽETAK

Metavalentne veze u dimerima metalnih elemenata u biomakromolekulama: pristup formiranja baza podataka s dodatnim primjerima podataka za srebro i kalij

Rudolf Kiralj *

Homonuklearni dimeri metala postoje u raznovrsnim oblicima, također i kao dijelovi biomakromolekulskih struktura. Cilj ovog rada je naći sve metalne elemente koji stvaraju takve dimere u Protein Data Bank (PDB), razjasniti strukturu i veze dimera raznim strukturnim deskriptorima i statističkim metodama te poduprijeti nove nalaze pomoću dvaju dodatnih istraživanja o klasterima srebra i kalija. Sveukupno je nađeno da 31 metal stvara 565 dimera u kristalnim strukturama biomakromolekula: metali *s*-bloka (Li, Na, Mg, K, Ca, Rb. Sr, Cs, Ba), prijelazni metali (V, Mn, Fe, Co, Ni, Cu, Zn, Mo, Ru, Rh, Pd, Ag, Cd, Au, Hg), metali *p*-bloka (Ga, Tl, Pb) te lantanidi (La, Eu, Dy, Ho). Ti nalazi čvrsto sugeriraju da svaki metal može stvarati dimere u biomakromolekulama. Pronađeni dimeri imaju metavalentne veze, ili granične metavalentne/kovalentne ili metavalentne/metalne veze. U PDB i drugim strukturnim bazama i literaturnim izvorima pronađen je 761 klaster srebra svih veličina, te su klasteri analizirani u smislu odnosa broja veza po atomu i odstupanja duljine veze. Metavalentne veze ili granične metavalentne/kovalentne ili metavalentne/metalne veze postoje u dimerima i malim klasterima srebra, dok je metalna veza dominantna u većim klasterima. Pretpostavlja se da drugi metali imaju ovakvo ili slično ponašanje. Odnos parcijalnog atomskog naboja i radijusa za 515 klastera kalija, koji su pronađeni u PDB bazi i u drugim bazama i izvorima, pokazuje da dimeri kalija u biomakromolekulama također imaju metavalentne veze ili barem granične metavalentne/kovalentne ili metavalentne/metalne veze, što je prilično jasno iz dijagrama raspršenja preneseni elektroni – dijeljeni elektroni. To je vrlo vjerojatno ponašanje i drugih metala.

Ključne riječi
Homonuklearni dimeri metala, biomakromolekulske strukture, metavaletno vezivanje, odnos veza po atomu i odstupanja duljine veze, odnos atomskog naboja i radijusa, odnos prenesenih i dijeljenih elektrona

Veleučilište u Bjelovaru,
Trg Eugena Kvaternika 4, 43 000 Bjelovar

Izvorni znanstveni rad
Prispjelo 25. kolovoza 2024.
Prihvaćeno 4. studenoga 2024.